6-28-2018

# Design and characterization of polymer nanocomposites for engineering applications

Joseph Richard Nalbach
*Rowan University*

# DESIGN AND CHARACTERIZATION OF POLYMER NANOCOMPOSITES FOR ENGINEERING APPLICATIONS

by

Joseph Richard Nalbach

A Thesis

Submitted to the
Department of Mechanical Engineering
In partial fulfillment of the requirement
For the degree of
Master of Science in Mechanical Engineering
at
Rowan University
May 23, 2018

Thesis Advisor: Wei Xue, Ph.D.

**Dedications**

I would like to dedicate this manuscript to my friends and family who have supported me, especially my mother and father, Dawn and Joseph A. Nalbach.

**Acknowledgments**

I would like to thank my advisor, Professor Wei Xue for his help and guidance, not just as I worked towards this accomplishment but also for the countless hours of help he provided during my undergraduate years. With knowledge and experience I acquired throughout working with him I was able to discover my passion for nanotechnologies.

Additional thanks Professor Robert Krchnavek, and Mr. Michael McCaffrey for their work and collaboration during the polyimide-$SiO_2$ cryogenic dielectric phase of my experiments.

Thank you to Naval Surface Warfare Center, Philadelphia and the Naval Engineering Educators Consortium program for the funding (Grant: N00174-17-1-0008) and assistance during the work done for polyimide-$SiO_2$ cryogenic dielectrics.

I would also like to thank Taissa Michel, without your love and support, I doubt I would have started on this journey.

**Abstract**

Joseph Richard Nalbach
DESIGN AND CHARACTERIZATION OF POLYMER NANOCOMPOSITES FOR ENGINEERING APPLICATIONS
2017-2018
Wei Xue, Ph.D.
Master of Science in Mechanical Engineering

Polymer nanocomposites represent an area of materials that can yield useful properties not achievable in bulk materials. Not only can they have such properties but also they can be relatively easy to generate. With dwindling fossil fuels there is an increased need for both new methods to harvest energy and to transport the captured energy more effectively. Two separate nanocomposite materials are created to support this work with dramatically different properties, both to aid in energy efficiency. The first is an energy harvesting foam to fully utilize the structural deformability of such a material. A dissolvable sugar scaffold is combined with ex-situ nanocomposite generation to generate an energy harvesting piezoelectric foam made from PDMS-ZnO-CNT. The second material is a cryogenic dielectric to potentially expand the capability of superconducting cables. An in-situ sol-gel method and a standard ex-situ method are both explored to create polyimide-$SiO_2$ dielectrics. The materials are tested with a variety of methods to characterize their structural, mechanical, and electrical properties. The piezoelectric foams yield a maximum electrical voltage of 0.30 V with a Young's modulus of 0.54 MPa and an ultimate tensile strength of 0.27 MPa. The dielectric material successfully withstands 34 kV/mm, and has a maximum tensile strength of 24.42 MPa at room temperature.

**Table of Contents**

**Table of Contents (Continued)**

**Table of Contents (Continued)**

## List of Figures

## List of Tables

# Chapter 1

# Introduction

## 1.1 Classic Materials

The basis of any gadget, part or system is the material from which they are made from. This singular choice can determine if and how well the object in question performs. For example, attempting to insulate high power transmission lines with paper will end in disaster, as while paper is an electrical insulator, it has an inhibiting low ignition point for such an application. The potential for such incidents is what makes material selection, and by extension material research so important.

In order to aid in material selection, classical materials are grouped together based upon their properties: metals, ceramics, polymers, and composites. Figure 1 illustrates examples of such materials.

Metals are materials that are identified by their metallic bonds. These materials are often viewed as the strongest, most desirable material from the standpoint of most of society. In truth, while metals tend to be more durable that other materials, there have been ceramics and composites that have shown higher strength values. In reality metals bring so much more than strength to the table; they have excellent conduction of both electricity and heat, and increased mechanical ductility over other materials [1]. Furthermore, metals are highly versatile and can be used for many other applications such as magnetic cooling, semiconductor technology and as antimicrobial agents [2-4].

Ceramics are often associated with pottery and art, however they represent a large section of useful engineering materials. In general ceramics are typically compounds formed between metallic and non-metallic components. They are classified by their high

corrosion resistance and electrical/thermal insulating properties. Due to these properties ceramics have been explored as thermal shielding in both nuclear power and solar energy systems [5, 6].

Polymers are created from repeating monomer chains [7]. They often have high dielectric properties, low melting points, and some corrosion resistance. Polymers have a wide range of applications, being used in sensors, electronic skins, energy harvesting, etc. [8-10].

Any material where two or more macroscopically identifiable base materials work together to achieve an enhanced result is considered a composite [11, 12]. Due to the hybridized nature of composites, they display a variety of different properties depending on what the "parent" materials are. These "parent" materials are referred to as the host material and the fill material. The quality of these materials is heavily dependent on the distribution and uniformity of filler in the host matrix [13]. Various host matrices and fillers have been explored in laboratory settings, such as reinforced concrete based composites [11]. In addition to using base materials made in laboratories, composites can also include natural materials such as wood [14].

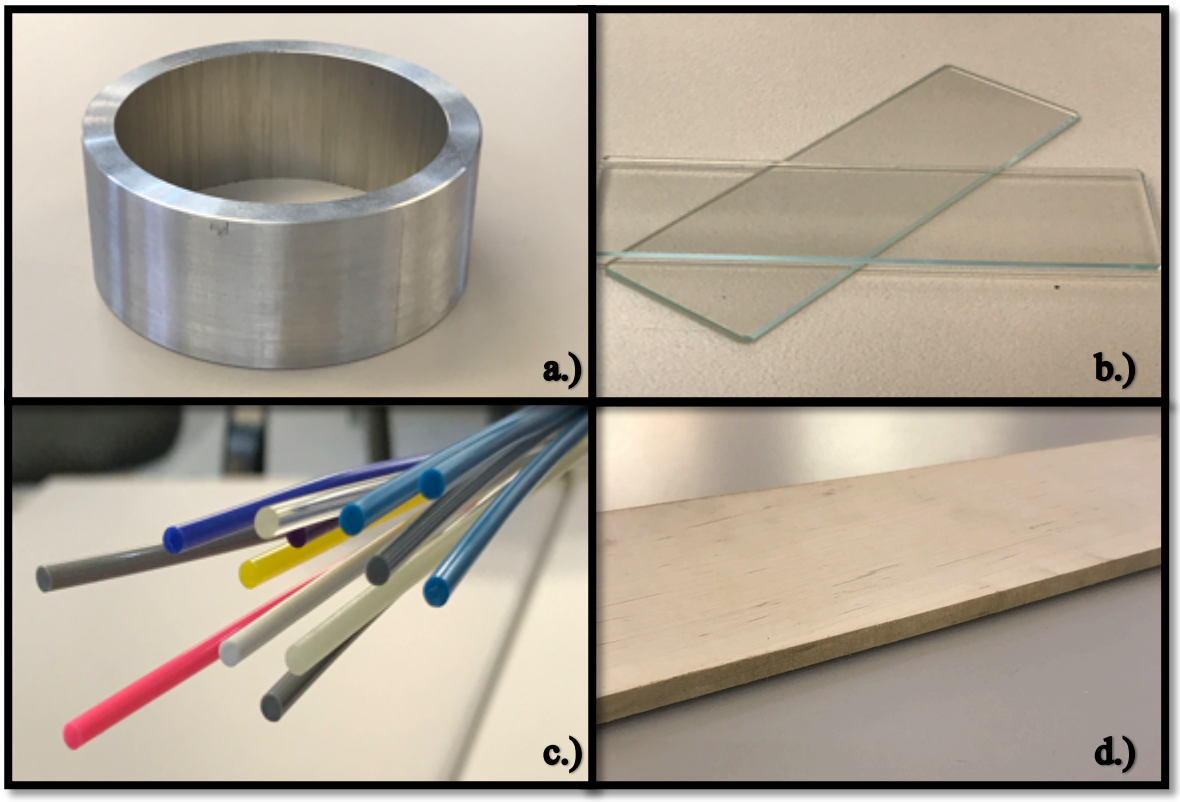


*Figure 1*. Common materials: a.) Aluminum is a common engineering metal. b.) Glass, a ceramic, is used for optical microscope slides. c.) Polylactic acid (PLA) is a plastic commonly used in 3D printing. d.) Plywood is a manmade resin/wood fiber composite for construction.

Additionally, the atomic structure of these arrangements also can significantly impact material properties. Carbon, for example, owes its properties to specific crystalline structures; it is capable of being the hardest known substance, diamond, or an material with lubrication properties, graphite [15, 16]. Variations of the same material only differing in atomic structures are called allotropes, and as previously stated can behave differently from each other [17, 18].

### 1.2 Polymer Nanocomposites

Nanocomposites are a form of composite materials that require one or more fillers at the nanoscale. The first generation of nanocomposites was reported in the early 1900s, and included efforts such as adding carbon black to rubber to create a material called Bakelite [19]. Despite this relatively early birth, these composites did not attract a significant amount of attention until the early 1990s when it was revealed that such fillers could dramatically reinforce a material [20, 21]. A visualization of a polymer nanocomposite is shown in Figure 2.

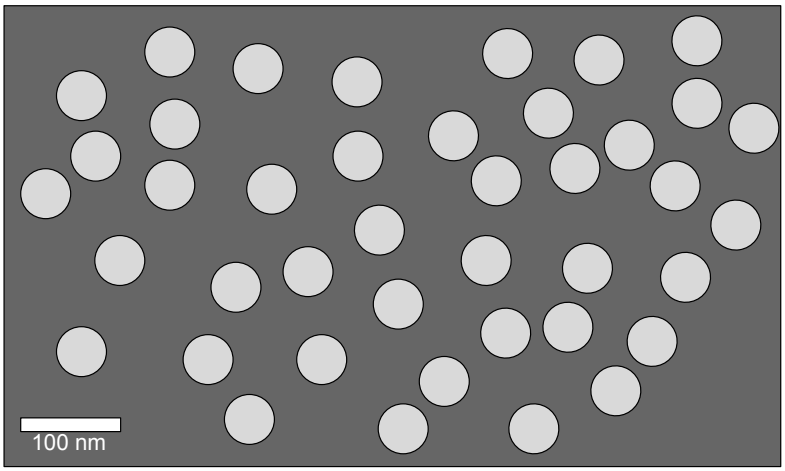


*Figure 2.* Visualization of nanomaterial filler within a host matrix. The dark gray region is the host matrix and the light gray regions are nanomaterial fillers.

### 1.3 Host Matrix

Part of the naming of nanocomposites lies in the category of host matrix, that is to say metals, ceramics, and polymers can all be used to generate nanocomposites. Two out

of the three host materials, polymers and ceramics, naturally lend themselves to the creation of nanocomposites. Metals however require specific processes to accomplish the same feat.

Polymer host matrices lend themselves naturally towards nanocomposite generation [22]. Using a liquid state polymer, nanomaterials can be easily added and mixed into the host material. The polymer is then cured, fixing the nanomaterials in their final placement within the composite.

One method of metal matrix nanocomposites, called stir casting, is incredibly similar to the process used to generate polymer-based nanocomposites. It essentially involves melting the metal down into a liquid state and adding a specific nanomaterial that has been pre-generated. The issues and other comparable methods have been reported in recent publications [23, 24].

Ceramics are also naturally receptive to nanomaterial generation as they often start as powders, later being fused together with the use of binding agents. Nanomaterials can be mixed into these powders to be distributed in the matrix. As the ceramic fuses together the nanofillers are locked in place.

### 1.4 Nanomaterial Fillers

A wide variety of nanoscale fillers have been explored including particles, fibers tubes, etc. [25-27]. These materials are typically sub 100 nm, placing them definitively in the realm of nanotechnology. At this size scale, Van der Waals forces cause particles to aggregate, creating a new filler distribution challenge for material scientists [28]. To combat this issue, two different methods of infusing the nanomaterials into a host have

been explored, ex-situ and in-situ [29, 30], exemplified in Figure 3.

In ex-situ methods, nanomaterials are first synthesized separately from the host matrix. These materials are then contained within a suspension in a host material compatible solvent or as a simple powder. They are then mixed into the host matrix as the filler. This method can be done quickly as half or all of the necessary components are already generated.

In-situ methods synthesize the nanomaterials within the host matrix. This can be done through various chemical processes. While the host materials are being stirred, these nanomaterials are formed, distributed and stabilized. This method is particularly compatible with the sol-gel method of nanoparticle synthesis, as the polymer host matrix functions as both the stabilizing and separating agents for the gel solution.

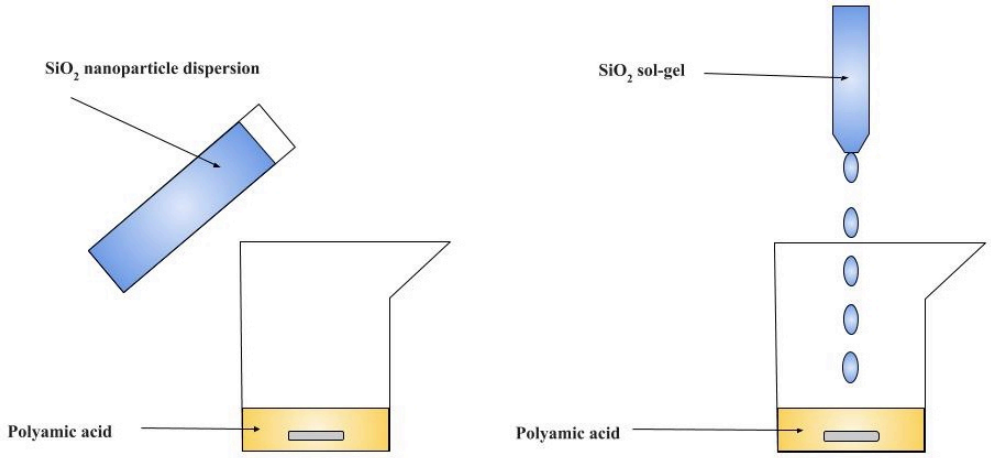


*Figure 3.* Ex-situ vs. in-situ addition of nanocomposites. In this example the in-situ method is based upon use of a sol-gel.

## 1.5 Applications

Nanocomposites can be used in almost all the same applications as other standard materials. Moreover, these nanocomposites offer additional, enhanced properties not typically demonstrated by their host materials.

One prominent area for nanocomposites is the aerospace industry, where nanostructures are used to create stronger and lighter materials to aid in modern flight airplane technology [31]. Another area where nanocomposites can heavily improve is battery technology. In this field such materials can be used to enhance the surface areas of anodes and cathodes, improving the battery life and performance [32]. The nanocomposites have also been used in medical research. There are numerous potential applications within this field ranging from tissue scaffolding to drug delivery. For example, nanoscale drugs can be infused into the human body via patches or nanoscale structures can be used to reinforce internal organs that have been damaged by prior injury [33, 34].

## 1.6 Motivation and Objectives

With dwindling fossil fuel reserves new methods of energy harvesting are becoming more important than ever. Various alternative energy sources can be exploited for energy generation, including humans. Humans produce a large amount of excess movement through basic locomotion, which can be potentially captured [35]. In addition to generating energy in new and responsible ways, increasing energy transport efficiency is of critical importance. In high power applications multiple cables are required to transport the requisite energy. Systems utilizing superconductivity represent one such

way to increase energy transfer efficiency with a high power load. However these systems suffer from the limited choice of dielectric materials that can withstand the cryogenic temperatures in a superconducting environment.

To that end the projects described in this thesis hope to accomplish the following:

- Develop a foam based material to capture human based energy
- Characterize the mechanical and electrical performance of such a material
- Develop a dielectric material for high temperature superconducting (HTS) cables
- Test the mechanical and dielectric strength of the composite at room temperature
- Design an environmental chamber to allow for future testing at cryogenic conditions

# Chapter 2

## Fabrication of PDMS -ZnO-CNT Foams Based Upon Sugar Scaffolds

### 2.1 Introduction

**2.1.1 PDMS foams.** Polydimethylsiloxane (PDMS) is a silicone-based rubber that has a wide variety of applications in research. It can be easily molded into a plethora of useful geometries and is commonly used in microfluidics, implantable devices, and composites as a host matrix [36, 37]. Its properties as a thermosetting plastic make it particularly receptive as the host matrix. In a general process, PDMS starts off as a liquid and solid fill materials are added later; the mixture is then cured into a solid structure through heating.

Foams come in two distinct forms: open pore and closed pore. Open pore foams have interconnected pores throughout the material, resulting in soft and springy structures. Closed pore foams are much stiffer as the air is trapped inside the pores without interconnectivity among these air pockets. Various efforts have been made to produce PDMS based foams, and accordingly a number of methods have been developed. One method is to use sugars as a dissolvable scaffold to create open pore geometries. Such sponges have been explored for separation of oil and water was well as for energy harvesting [38, 39]. As PDMS is an electrically insulating material, an additional fill needs to be added to make the material more conductive for harvesting applications.

**2.1.2 Carbon nanotubes.** Carbon nanotubes (CNTs) belong to a special group of carbon allotropes called fullerene structures; all of which exist at a nanoscale [40]. Interestingly with carbon nanotubes, only their diameters are restricted to nanometers and their lengths can reach several millimeters. The structure of these tubes can be visualized

as a rolled sheet of carbon atoms bonded in a hexagonal pattern (this sheet being another popular nanomaterial, graphene). Carbon nanotubes have strong conductive properties for both heat and electricity, and as such are an excellent choice of fill material for conductive composites [41].

CNTs owe their unique properties to the crystalline arrangement of carbon atoms; their electrical properties can be altered by changing the orientation of these atoms. The type of CNT formed is determined by how the graphene sheet is rolled. For example, for the carbon sheet shown in Figure 4, rolling in the direction of the vertical arrow yields an armchair CNT, whereas following the horizontal vector results in a zig-zag CNT. Any angle in between is known as a chiral, with a variety of notations to indicate the roll angle.

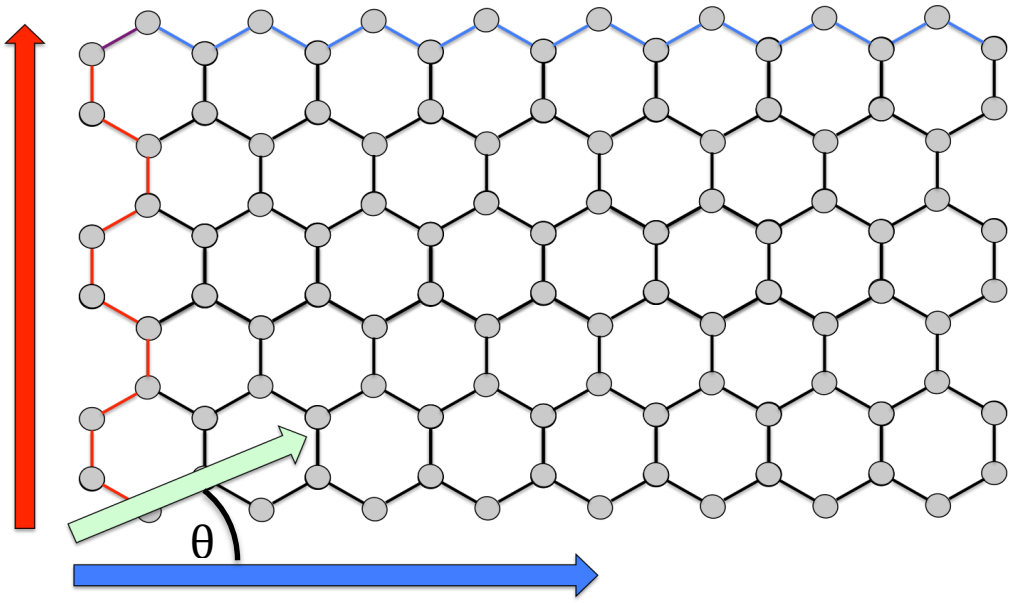


*Figure 4.* Chirality map of a CNT

**2.1.3 Energy harvesters.** The rise in fossil fuel consumption has led to an increased need for alternative energy [42]. New energy harvesters using photovoltaic, thermoelectric, and/or piezoelectric properties have been developed. For example, solar panels, one of the most commonly used energy harvester converts light into electricity, using photovoltaic cells. Likewise, thermoelectric harvesters convert a temperature difference into an electrical output, and piezoelectricity takes mechanical deformation and converts that into electrical energy [43].

Piezoelectricity is unique in that all sources of forces, including human locomotion, can induce mechanical deformation, which in turn can be converted to electrical energy. This means that electronic devices, such as phones, could potentially be charged by the everyday activity of the users [44, 45]. This provides an opportunity that everyday items can potentially be infused with electrical producing traits for energy generation. One item that particularly experiences repeated deformation is the foam soles of shoes. If a foam could be enabled with piezoelectric properties, the simple act of walking can generate electrical outputs.

**2.1.4 Piezoelectric materials.** In order to obtain piezoelectric properties, the fill material must be inherently piezoelectric, such as lead zirconate titanate (PZT), zinc oxide (ZnO), polyvinyl difluorine (PVDF), and barium titanate ($BaTiO_3$) [46, 47]. Both zinc oxide and barium titanate are available as nanoparticles; making them suitable materials as fillers for nanocomposites; PVDF can be electrospun into nano and microfibers as potential filler structures.

## 2.2 Material Preparation

The basis of generating the energy harvesting foams is to combine a liquid thermosetting nanocomposite over a dissolvable sugar scaffold. Three types of sugar, granulated, brown, and ultrafine sugars, were used and compared over the course of the study.

**2.2.1 Preparation of the composite.** The nanocomposite generated in this study used PDMS (Sylgard 184) as the host matrix through an ex-situ method. It was prepared by combining ten parts of elastomer component with one part of curing agent. These two materials were combined and mixed until a uniform consistency was obtained. The nanomaterials were weighed and mixed into the PDMS. The ZnO nanoparticles, purchased from Nanoamor, were lipophilic and silicone oil coated to aid in dispersion. Multiwall carbon nanotubes (MWCNTs) were also purchased from Nanoamor. First, 10-wt% of ZnO nanopowder was measured out and placed in a weigh boat. Then 1-wt % MWCNT powder was also measured and added to the same weigh boat. The two powders were mixed together until the result was homogeneous. The mixed homogeneous powder was then carefully added to prior prepared PDMS.

*Figure 5.* Completed PDMS-ZnO-CNT nanocomposite before it is combined with the scaffold.

**2.2.2 Use of scaffolds.** Both granulated and ultrafine sugars could be used to generate foamed structures in the exact same manner. First, 40 mL of the sugar is measured in a graduated cylinder. The sugar was then mixed with 18.3 g of the PDMS-ZnO-CNT nanocomposite to form a moldable non-Newtonian fluid, with the rough consistency of clay. This mixture is packed into glass petri dishes to act as molds. The molds were cured on a hot plate at 60 °C overnight to cure to a solid phase.

The cast was then released from the mold and place in a bath of boiling water. This process removed the sugar content and the resulted structures were left in the bath until all of the sugar was removed, typically 24 hrs. The result was a disc-shaped foam that could be cut into various samples.

Brown sugar has molasses inside; because of this added content, brown sugar had to be handled differently from the other two, as illustrated in Figure 6. First, 40 mL of brown sugar was packed into a petri dish, and then 18.3 g of PDMS-ZnO-CNT nanocomposite was slowly poured over the top, carefully not to overflow. Afterwards, the partially soaked composite-sugar mixture is place in a vacuum chamber for 2 hr to allow complete filling of the composite through the scaffold. The final mold was cured on a hotplate over night at 60 °C. As with the other sugar scaffolds, the cured sample was placed in a dissolution bath until the sugar had been completely removed.

For all sugar scaffolds the final foams were cut into geometrically controlled samples measuring approximately 2.5 cm × 1.5 cm × 1.5 cm.

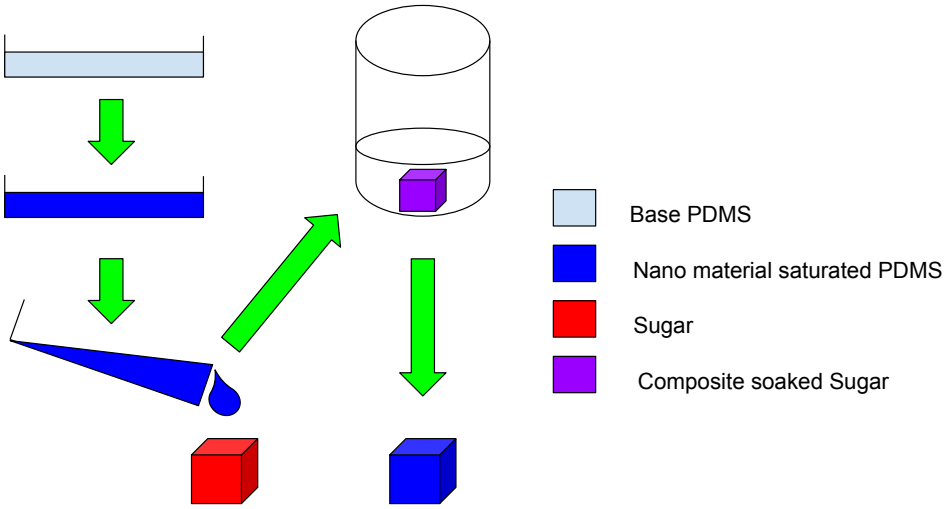


*Figure 6.* Process flow of leaching process to generate nanocomposite foam.

**2.3 Discussions**

Visual inspection indicated that out of the three sugars selected, only two produced reliable foams; ultrafine and granulated. For the successful methods, ultrafine was determined to be more desirable than the granulated sugar as it yielded smaller pore sizes, pictured in Figure 7.

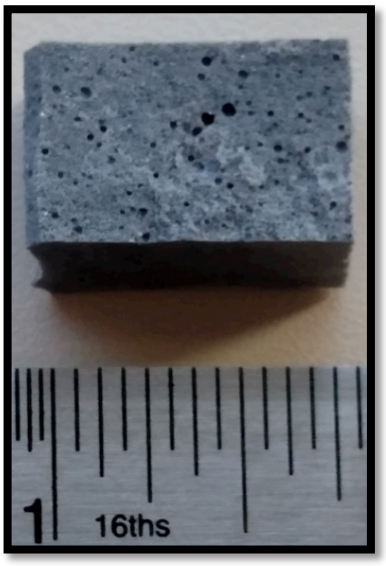


*Figure 7*. Completed piezoelectric sponge material cut into a rectangular prism.

# Chapter 3

## Characterization PDMS-ZnO-CNT Foams Based Upon Sugar Scaffolds

The material created in Chapter 2 was subjected to physical, mechanical, and electrical testing to better understand their materials properties.

### 3.1 Physical Characterization

Scanning electron microscopy (SEM) was used to determine the pore diameter and distribution. SEM characterization of the resulting foams is carried out using a desktop Phenom SEM. Inspection of samples was used to obtain the size information of the pores. Figure 8 shows clear differences between the size and distribution of the pores within the material from different scaffolds. Samples generated from brown sugar have pores that are randomly distributed and have no consistency in terms of diameter and pore volume, as shown in Figure 8a. Ultrafine sugar scaffold creates pores with a much higher degree of consistency in terms of pore diameter and distribution (pore diameter 50 - 150 μm), as shown in Figure 8b.

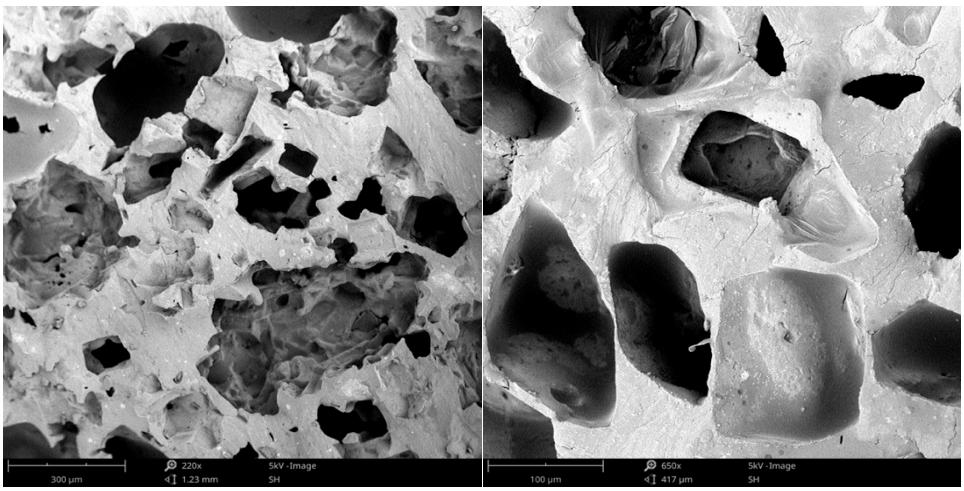


**a.)** **b.)**

*Figure 8.* a.) Brown sugar sponge with large pore variations, shown at a scale bar of 300 µm. b.) Ultrafine sugar sponge with more uniform pore sizes and distribution, shown at a scale bar of 100 µm.

### 3.2 Mechanical Characterization

The mechanical strengths of piezoelectric foams are of critical importance, therefore tensile testing was performed on the generated foams using a tabletop SHIMPO MTS (Material Testing) system.

The mechanical properties of all the tested samples are illustrated in Figure 9. Samples show high linearity between stress and strain, an expected result as the host polymer PDMS is a well-known elastomer. The solid PDMS-ZnO-CNT sample remains elastic for the entire testing range. The Young's modulus, ultimate stress, and ultimate strain are calculated as 4.40 MPa, 0.75 MPa, and 18.79%, respectively. The ultrafine sugar sponge shows mostly elasticity in its stress-strain curve with slight plastic deformation beyond the ultimate strength point. The Young's modulus, ultimate stress, and ultimate strain are calculated as 0.54 MPa, 0.27 MPa, and 57.33%, respectively. The

statistical comparison of the Young's moduli for the four samples is shown in Figure 9c. All three sponge samples exhibit similar values (averaging 0.54 MPa for granulated, 0.50 MPa for brown, and 0.44 MPa for ultrafine sugar foams). They are significantly softer than the solid film sample (averaging 4.40 MPa for its Young's modulus). The differences for the foams are much more pronounced when comparing their ultimate tensile strengths, as illustrated in Figure 9d. All three foam samples are weaker than the solid film, which has an average strength of 0.74 MPa. The ultrafine sugar sponge is the strongest among all the foamed samples with 0.28 MPa for its ultimate strength, followed by the granulated sample with 0.21 MPa and brown sugar sponge with the lowest strength of 0.16 MPa.

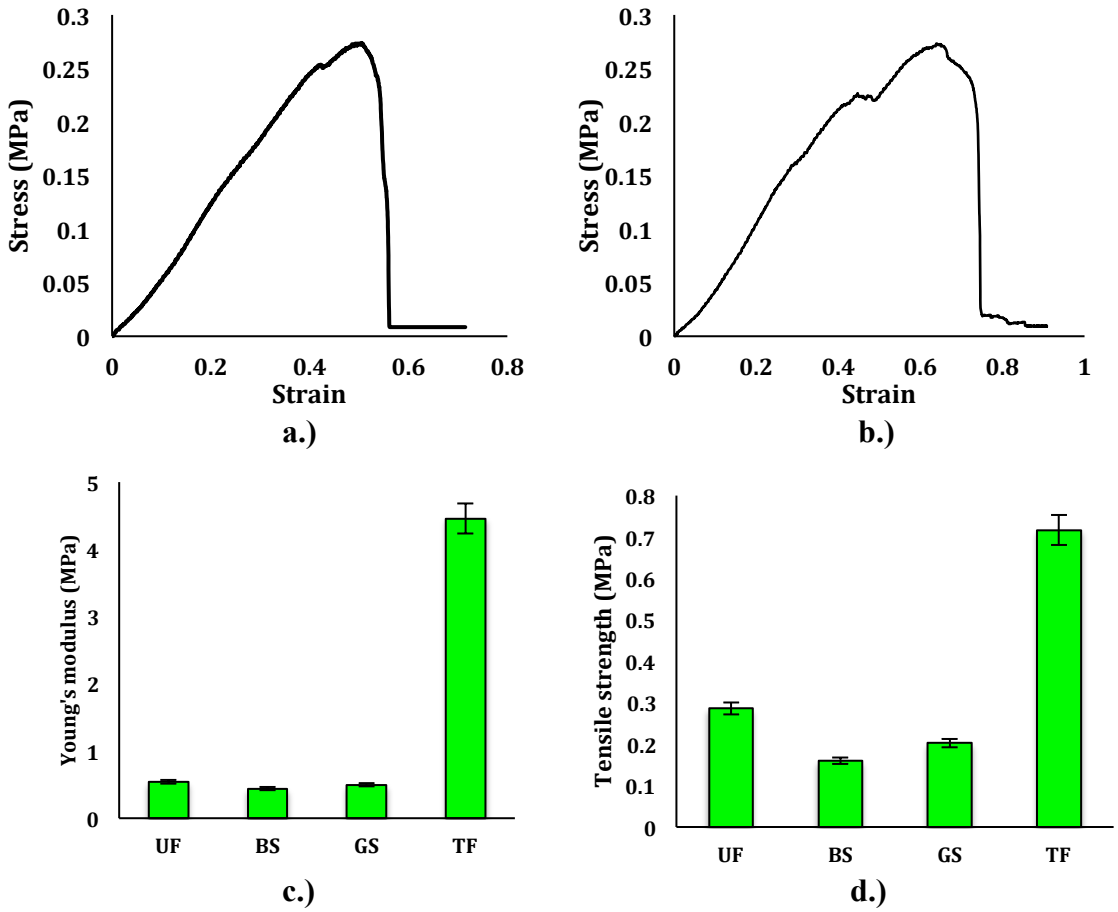


*Figure 9.* a.) Stress-strain curve of a granulated sugar sample. b.) Stress-strain curve of an ultrafine sugar sponge. c.) Histogram comparing Young's moduli of all samples. d.) Histogram comparing ultimate tensile strengths of the samples. UF: ultrafine sugar; BS: brown sugar; GS: granulated sugar; TF: thin film.

### 3.3 Electrical Characterization

One of the most desirable properties for these foams is the electrical output under mechanical stresses. The electrical properties of each sample are obtained and analyzed through the use of an integrated mechanical-electrical testing system and a data acquisition device. The system setup is illustrated in Figure 10a and the process flow is shown in Figure 10b. The testing system is used to apply a controlled loading to the

sample, and at the same time measure the generated electrical signals via the DAQ and a data acquisition LabVIEW code. A waveform generator creates a controllable sinusoidal signal. This signal is then amplified using a signal amplifier, resulting in testing values of 30 Hz and the peak-to-peak voltage is 240 mV. This amplified signal is passed to an electrodynamic shaker. A thick, rectangular acrylic plate is bolted on the shaker's surface with one end cantilevered out to provide a tapping head. The sample is mounted on another acrylic plate and placed directly underneath the cantilevered tapping head. During testing, the vibration generator applies vertical forces to the sponge sample and deforms it. The two copper leads from the sample are connected to the DAQ to collect the voltage produced by the mechanical deformation. The LabVIEW code records the oscillating voltage output from the sponge sample and display the signal on a computer monitor. The measured results are saved for data evaluation.

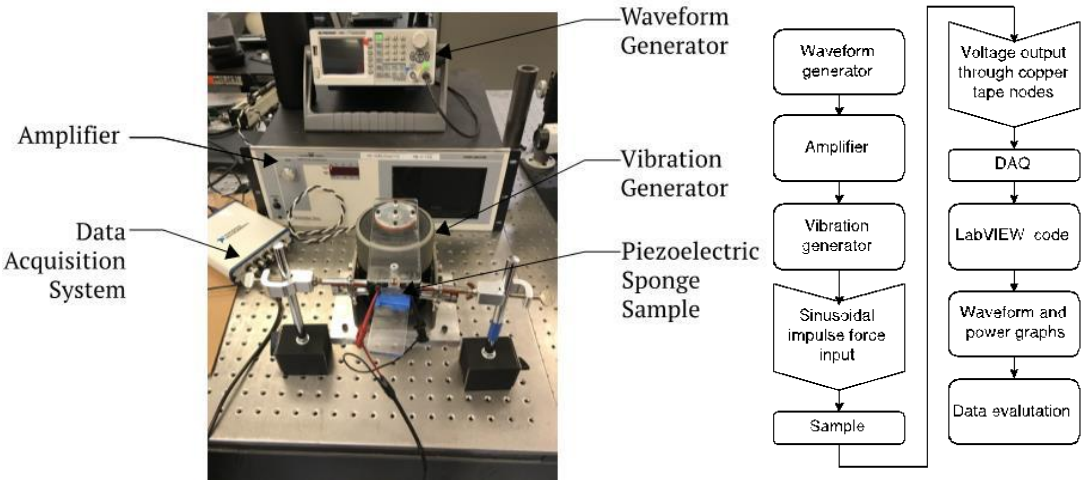


**a.)** **b.)**

*Figure 10.* a.) Electrical testing set up. b.) System flow of electrical testing set up.

Even without electrical poling, all the samples exhibit clear piezoelectric behaviors during the integrated mechanical-electrical testing. The electrical output of a solid PDMS-ZnO-MWCNT film under controlled mechanical vibration is shown in Figure 11a. The peak-to-peak voltage is approximately 0.03 V. By comparison, an ultrafine sugar sponge shows a higher peak-to-peak output voltage of 0.30 V, as shown in Figure 11b.

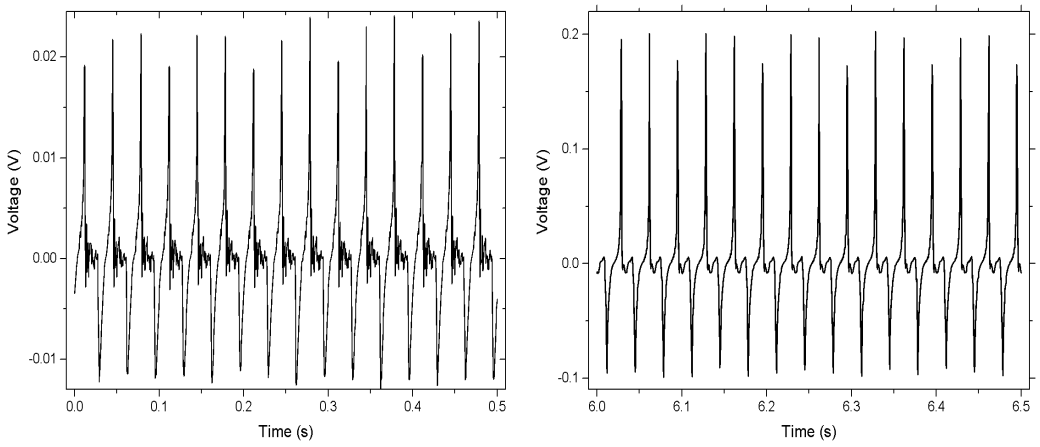


**a.)** **b.)**

*Figure 11.* Sample data generated by the electrical testing set up for a.) a brown sugar based sample generating approximately 0.03V and b.) an ultrafine sugar based sample generating 0.3 V, an increase of an order of magnitude .

Figure 12 compares the output voltage performance for the four samples. The ultrafine and granulated sugar samples show clear electrical performance enhancement from the solid films. It is expected that such enhancement is a result of larger structural deformation of the foamed samples. As all the samples are tested under the same

condition, the amount of structural deformation for each sample is determined by its mechanical properties. For a foamed structure, the lower Young's modulus and the porosity allow it to be stretched/compressed further than a solid film. For the brown sugar sponge, however, its performance is only comparable to that of the solid films. We suspect that the size and variability in their pore distribution cause a weakened framework, which in turn reduces the connectivity of ZnO and MWCNTs. As a result, the generated electrical charges under stress cannot be transmitted to the electrodes effectively.

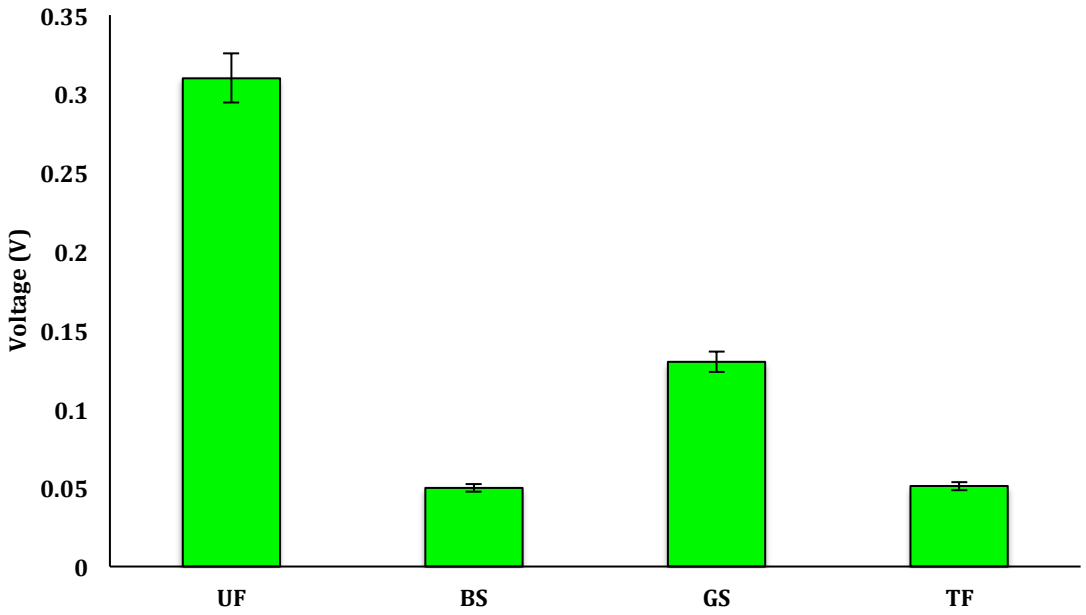


*Figure 12.* Histogram illustrating peak-to-peak voltages produced by each foaming method and a film specimen.

Table 1 summarizes all the important parameters related to the four samples. As a group, the nanocomposite foams demonstrate lower density and higher flexibility; both of them are desired properties for portable technology. Their tensile strengths are reduced but still have sufficient strength to allow for the material to be deformed repeatedly without mechanical failure. The more interesting property of these foams is their enhanced mechanical-to-electrical conversion performance. The larger deflection these foams experience during loading leads to higher piezoelectric responses. However, there appears to be a limit to this phenomenon, mostly affected by the porosity for the foamed structure. For example, the brown sugar sponge has the lowest density and Young's modulus; its piezoelectric response, however, is the weakest of all the tested samples. The ultrafine sugar sponge demonstrates some of the properties suitable for piezoelectric energy harvesting applications. Based on the SEM inspection, it is believed that the porosity of the foamed structures plays a critical role in their overall performance, as samples with large voids and gaps in the porous structure (e.g., brown sugar samples) produced low mechanical and electrical values.

Table 1

*Summary of critical parameters for the tested samples*

| Sample | Density ($g/cm^3$) | Young's Modulus (MPa) | Tensile Strength (MPa) | Electrical Output (V) |
|---|---|---|---|---|
| Granulated Sugar Sponge | 0.97 | 0.50 | 0.21 | 0.13 |
| Brown Sugar Sponge | 0.60 | 0.44 | 0.16 | 0.05 |
| Ultrafine Sugar Sponge | **0.95** | **0.54** | **0.28** | **0.30** |
| Solid Film | 1.08 | 4.40 | 0.74 | 0.05 |

### 3.4 Conclusions

The fabrication and characterization of PDMS-ZnO-MWCNT nanocomposite foams, which can be used as piezoelectric energy harvesters, has been explored. Three different types of foams are prepared using commercial sugar products as the scaffolds. Compared with other flexible piezoelectric materials, the foams have porous structures that allow for larger mechanical deformation of the samples, resulting in more efficient mechanical-to-electrical energy conversion. The foamed structures have a significant impact, both mechanically and electrically, on device performance. Our results demonstrate that the ultrafine sugar based foams are light and flexible. More importantly, they can generate peak-to-peak voltages of 0.3 V, approximately an order of magnitude higher than solid films composed of the same materials. Due to time constraints, current values are not obtained but will be investigated in future experiments. The fabrication process to prepare the samples is simple, fast, and inexpensive. The soft nature of these materials makes them great candidates as flexible energy harvesters for portable or

wearable devices. These new foamed materials will provide high potential in a wide range of applications that can benefit from their unique mechanical and electrical properties.

# Chapter 4

## Fabrication of Polyimide-$Sio_2$ Cryogenic Dielectric

Chapters 4-6 discuss the generation and testing of a dielectric material for cryogenic applications specific to Navy vessels. These applications largely surrounded power transfer on large naval ships, such as carriers and destroyers.

### 4.1 Introduction

Superconductivity is a quantum mechanical phenomenon where certain materials gain an increased current capacity when they are cooled to their respective transition temperatures [48]. Materials such as magnesium diboride and $LnNi_2B_2C$ become superconductive once they reach their transition temperature [49, 50]. The exact mechanisms leading to superconductivity are beyond the scope of this thesis and will not be discussed.

High temperature superconducting (HTS) cables are somewhat of a misnomer; despite being referred to as high temperature, they require temperatures slightly higher than that of liquid nitrogen (77ºK). However lowering the temperature further would increase the current density and the overall energy capacity. The HTS cables often use the three phase power setup, containing a cable core, three sets of superconducting elements and dielectric layers in between [51], as shown in Figure 13. Replacing liquid nitrogen with gas helium (melting temperature 4.2 ºK) as the cryogen allows for lower temperatures but also introduces new problems.

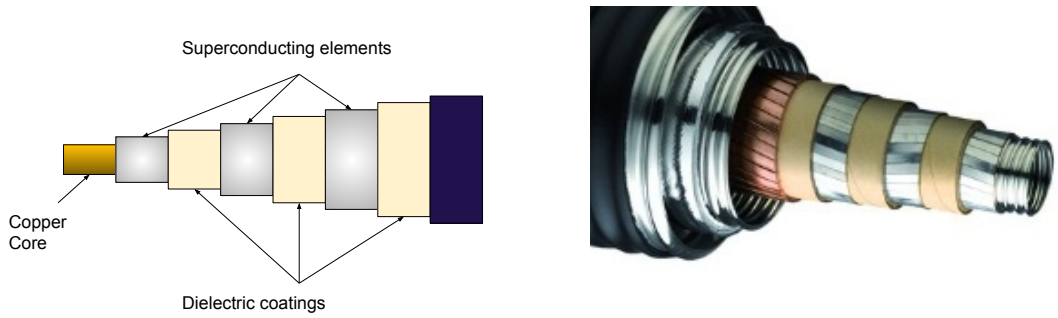


**a.)** **b.)**

*Figure 13*. a.) Illustration of the structure of a three-phase HTS cable. b.) A typical three phase HTS cable from Nexans (Image courtesy of Nexans Inc.).

Two critical issues occur: the first is that the overall dielectric strength of the cryogenic system decreases dramatically in gas helium, the second is that the coefficient of thermal expansion (CTE) of polymers is dramatically different than those of metals, causing CTE mismatch [52]. Dielectric strength refers to how much voltage a material can experience before the material fails. This failure not only allows electrical current to flow through but also results in structural defects in the material [53]. CTE mismatch results in one material expanding or shrinking more than the other material. This in turn results in gaps or holes in the final structure. Efforts have been made to minimize this problem using lapped dielectric tape; however helium's small atom size (0.49 Å) allows them to permeate through the small, approximately 100 μm gaps (called butt gaps) in the lapped tapes[54]. Due to the low dielectric strength of helium, electricity is able to conduct through the helium atoms; this lowers the overall dielectric strength of the tape [55-57]. Figure 14 illustrates these issues. A potential solution to these problems is to create an extruded polymer or polymer composite with a suitable dielectric strength (> 12

kV/mm) and a CTE that matches that of copper, the core cable material.

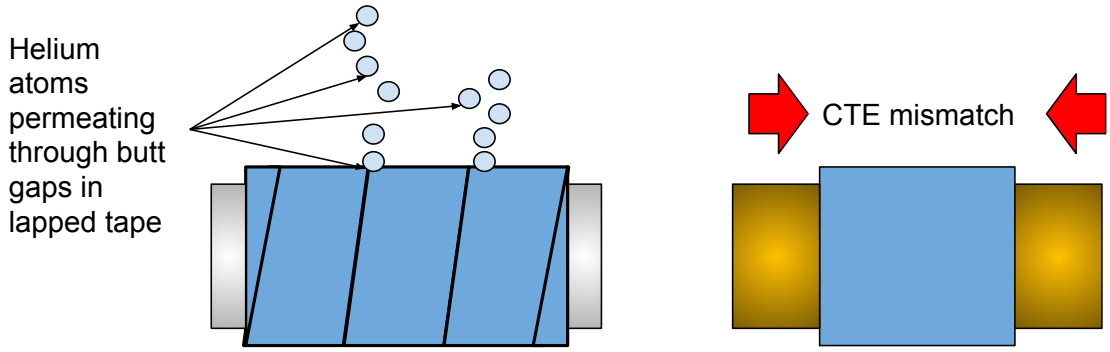


**a.)** **b.)**

*Figure 14*.a.) Helium permeating through butt gaps in lapped dielectric tape. These gaps have a typical diameter of 100 µm. b.) CTE mismatch between the copper core and the extruded polymer.

### 4.2 Material Preparation

A number of recipes were created and tested in order to optimize the electrical and mechanical properties of polymer composites. Previous work has explored host matrices of epoxy and polymers [58, 59] as well as various nanoparticle fillers including $SiO_2$, $TiO_2$, etc. [60, 61]. These past efforts have looked at dielectric breakdown strength, showing a range of values from 65 kV/mm to 145 kV/mm [62, 63].Table 2 summarizes various material process recipes used in recent publications.

Table 2

*Summary of reported process recipes and materials*

| # | Chemicals | Solvent | Chemicals | Citation |
|---|---|---|---|---|
| 1 | Diglycidyl etherof bisphenol-F<br>Diethyl toluene diamine (DETD)<br>Ammonia solution | Acetone | Polypropylene glyco ldiglycidyl ether (PPGDE)<br>Tetraethylorthosilicate | [59] |
| 2 | Araldite® CY 5808<br>BTO | | Hardener HY 5808<br>CCTO | [62] |
| 3 | Al fibers<br>Polyvinylpyrrolidone (PVP)<br>Tetraethoxysilane (TEOS) | | Al Particles<br>Polyimide Powder | [64] |
| 4 | Pyromellitic dianhydride (PMDA)<br>Tetraethoxysilane (TEOS)<br>Polyamic acid (PAA) | N,N-dimethy-lacetamide<br>Ethanol | Diphenylene diamine (ODA)<br>Hydrocholoric Acid | [61] |
| 5 | poly(methylmethacrylate) (PMMA),<br>Araldite® CY 5808<br>Barium titanate<br>Cobalt iron-oxide barium difluoride | | Polyvinyl alcohol (PVA)<br>Hardener HY 5808<br>Titanium dioxide | [58, 65] |
| 6 | N-Methyl-2-pyrrolidone (NMP, 99%)<br>Triethylamine (99%<br>KBr (99%)<br>Tetraethylorthosilicate (TEOS, 96%)<br>(3- tri-methoxysilylpropyl)<br>Diethylenetriamine | Ethanol | Polyamic acid solution<br>Phthalic anhydride (99%) | [66] |
| 7 | Araldite® CY 5808<br>TiO2 | | Hardener HY 5808 | [60] |

**4.2.1 Preparing host matrix.** The polyimide generated in this study was a condensation of pyromellitic dianhydride and diphenylene diamine. This was the case for both the commercially available polyimide and the home synthesized form. The commercial produce, 15 wt.% poly(pyromellitic dianhydride-co-4,4'-oxydianiline) amic acid solution, or short as poly(amic) acid (PAA), was purchased from Sigma Aldrich. Drying the as-purchased PAA on a hot plate at 70 ºC for 6 hrs evaporates the amic acid solvent and results in a polyimide film. We also investigated the synthesis of PAA in house. In this process, 1:1 molar stoichiometric quantities of pyromellitic dianhydride (PMDA), diphenylene diamine (ODA), and N,N-dimethylacetamide (DMAC) were mixed. First, the desired amount of ODA was fully dissolved in the DMAC solvent. Then one third of the required amount of PMDA was added every 20 minutes, over the course of 1 hour. The mixture turned into a viscous material that could be further dried to polyimide. However, our synthesis process results in inhomogeneous materials unsuited for further processing. This is due to the ambient environment used in our experiments, causing the material to oxide during the process. Based on other reports, a nitrogen environment would be required to produce high-quality polyimide solvent [61]. Comparing the two materials (as-purchased vs. in-house synthesized), we decided to focus on using the commercial PAA for further material processing.

**4.2.2 In-situ generation.** The nanoparticle synthesis method was based upon a popular sol-gel method [61]. The method was relatively simple as stoichiometric quantities of four chemicals, tetraethoxysilane (TEOS), hydrochloric acid (HCl), ethanol, and deionized (DI) water were mixed in a 250 mL beaker. To make the synthesis easier, the stoichiometry was converted to mass percentages of the total sol-gel solution. This resulted in 67.5 % TEOS, 11.8% HCl, 14.9 % ethanol, and 5.8% DI water, all by mass.

$$1\ mol\ TEOS * \frac{208.3\ g\ TEOS}{1\ mol\ TEOS} = \frac{208.3 g\ TEOS}{total\ gel\ mass} = 67.5\%$$

This calculation is used to determine the mass percentages of all the chemicals. The contents were placed in a beaker and stirred with a magnetic stirring rod at 150 RPM for 30 minutes before it became usable, shown in Figure 15.

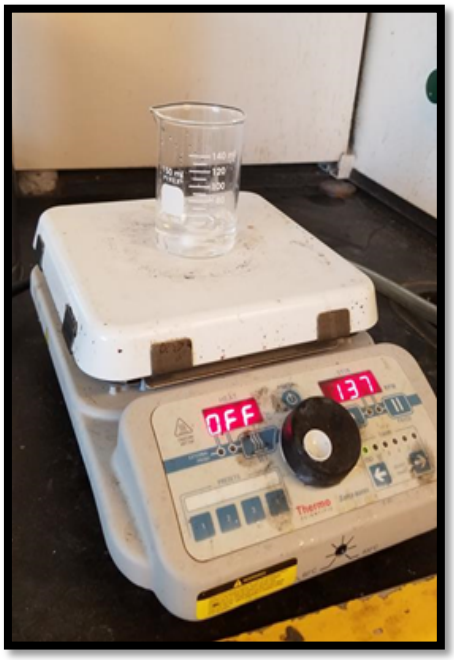


*Figure 15.* $SiO_2$ sol-gel being generated in a fume hood.

The in-situ method requires that the mass of the sol-gel matches the required weight percentage of the final composite. To stabilize the nanoparticles within the host matrix, the sol-gel is dropped into the polyamic acid three separate times in the course of an hour, 20 min apart, while the polyamic acid is stirred with a magnetic bar at 150 RPM. During this time, the excess sol-gel must be continuously stirred with a magnetic stirring bar to prevent it from turning solid. Once all the sol-gel is used, the entire mixture is stirred for 6 hours.

**4.2.3 Ex-situ method.** For ex-situ methods, a certain weight percentage of nanoparticle powder is dispersed in DMAC, 15 mL per 20 g of nanoparticles. To break up larger scale aggregates, the dispersion is subjected to ultra-sonication for 30 min. The dispersion is then immediately added to the polyamic acid in its entirety, and mixed for 6 hrs.

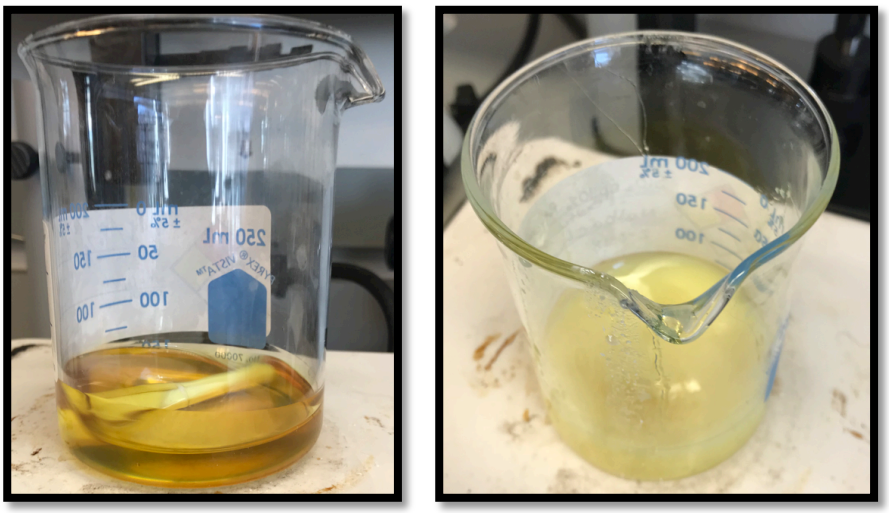

**a.)** **b.)**

*Figure 16.* a.) In-situ method being generated b.) Ex-situ method being generated. The ex-situ method produces a noticeably paler color in the liquid state polymer.

For both generation methods, once the mixing was complete (shown in Figure 16), the samples were converted into films for testing. To do this the liquid state composite was spun coat onto glass slides at 1500 RPM and cured at 70ºC for 30 min on a hot plate. The final films could then be separated from the slides, approximately 25 mm × 20 mm, and are ready to be tested, as pictured in Figure 17.

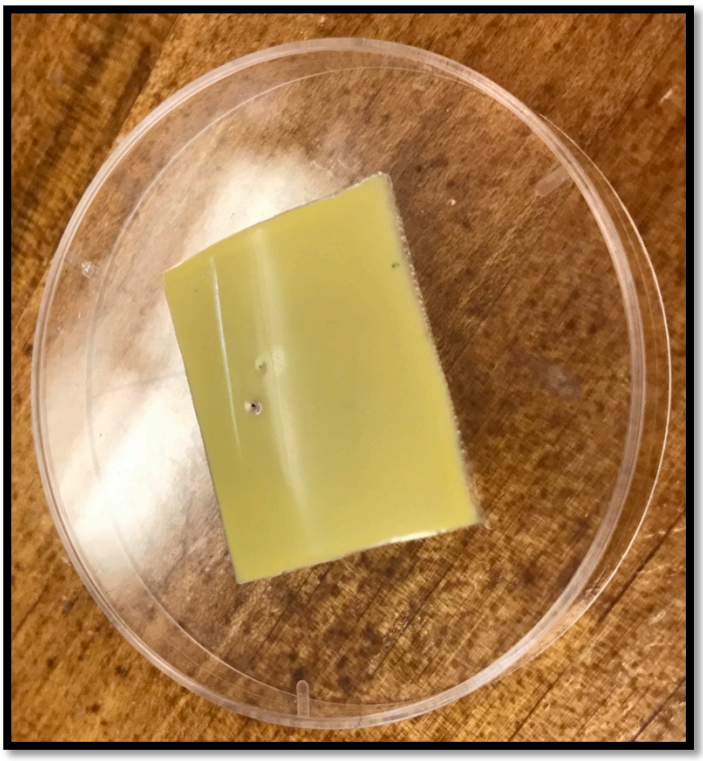

*Figure 17.* Film sample of a 10% in-situ recipe. The film was separated from a standard 1" × 3" glass slide.

### 4.3 Discussions

Both the ex-situ and in-situ methods produced films that could be separated from their substrates. However this success was limited to films made with as-purchased PAA. Due to the high level of oxidation experienced in the synthesis of PAA, the host material was brittle and could not be separated from the glass. This led to our decision of focusing only on as-purchased PAA as the host matrix. A nitrogen environment could be required to prevent such oxidation.

## Chapter 5

## Characterization of Polyimide-$Sio_2$ Nanocomposites

The materials generated in chapter 4 were subjected to room temperature testing. Specifically, pure polyimide samples and two types of composite samples (10-wt.% of $SiO_2$ in polyimide and 15-wt% $SiO_2$ in polyimide) were characterized. SEM inspection, tensile testing and electrical breakdown testing were performed to characterize the materials.

### 5.1 Physical Characterization

**5.1.1 SEM inspection.** Before SEM inspection could be performed, special steps needed to be taken. Due to the high dielectric nature of the material being imaged, electron charging and drift severely distorted the desired image. To combat this, selected samples were bonded to the SEM stub using copper tape. The stub was then sputtered with gold to provide a more conductive surface to aid in discharging electrons. The final step of preparing the stub was to cover the top of sample with more copper tape to save for only a small viewing window and make a connection to the back of the stub. Based on SEM inspection, particles of approximately 10 μm are observed in the in-situ sample, as shown in Figure 18. The particles were distributed relatively uniformly, but were much larger than expected. Upon further magnification, particles of approximately 15-30 nm were observed with an even distribution, as shown in the Figure 18b.

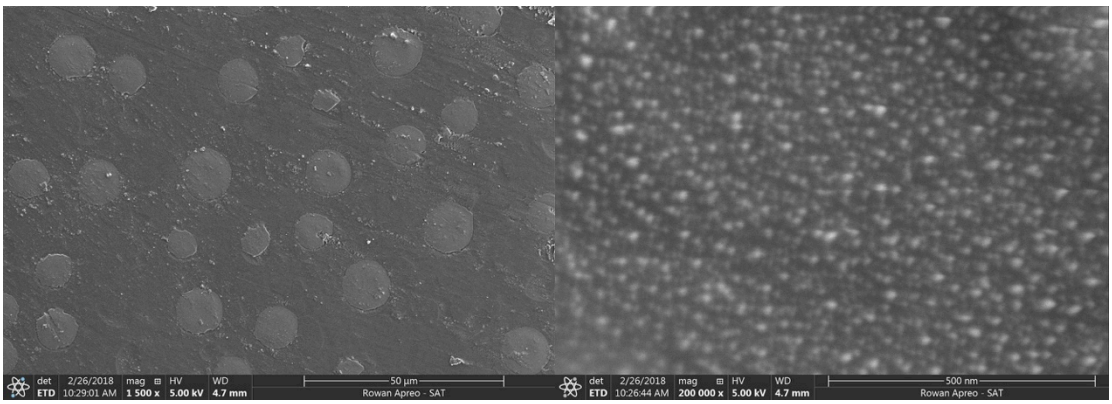


**a.)** **b.)**

*Figure 18.* a.) Micro particles evenly distributed in a 15-wt % sample. The micro particles are approximately 10 µm in diameter. b.) Nanoparticles evenly distributed in a 15-wt % sample. The particles measure approximately 20 nm.

For ex-situ samples, individual particles could not be observed, rather a continuous surface comprised of aggregates was revealed. This creates a rough surface topography not typically desired in nanocomposite generation. The surface topography can be viewed in Figure 19. Based on the SEM inspection, the samples from the in-situ method showed smoother topography and more uniform particle distribution. Therefore, they are selected for mechanical and electrical testing. Further investigations on the ex-situ method and the resulted samples will be needed in the future.

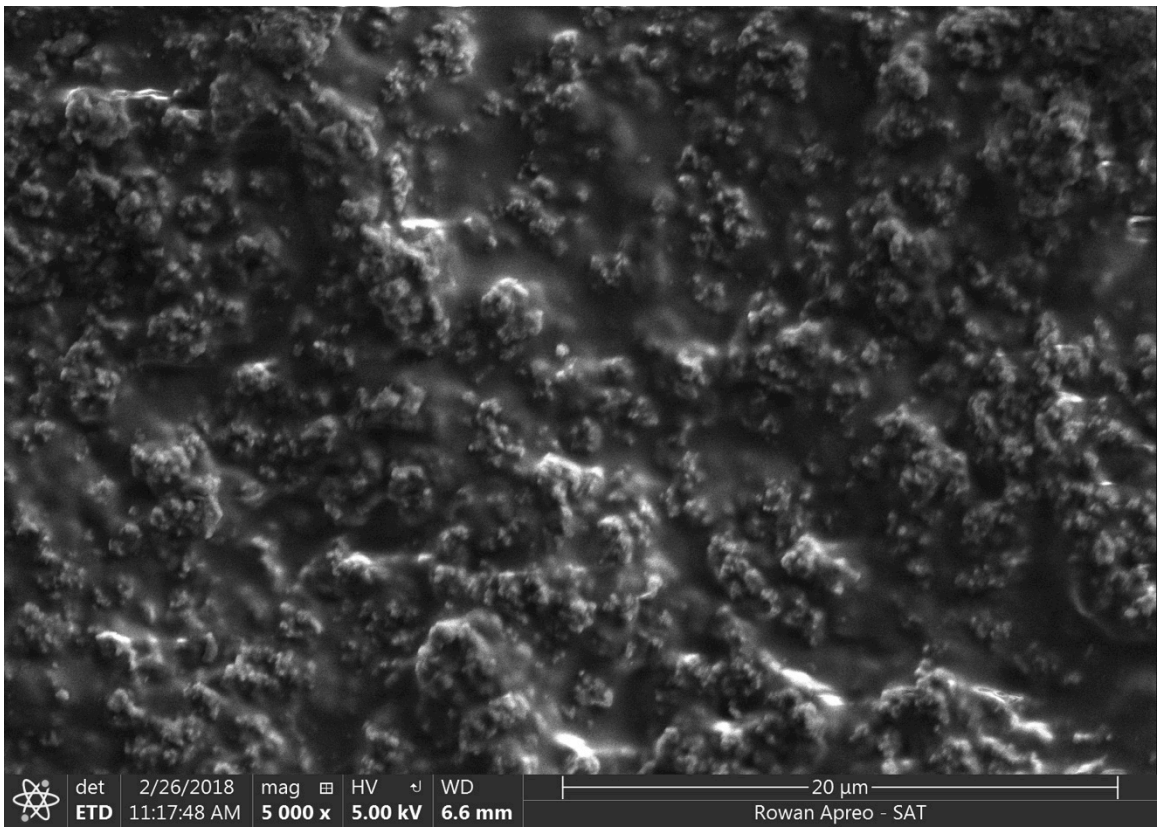

*Figure 19.* SEM image of an ex-situ sample. Individual particles are poorly defined and contained in aggregates.

**5.1.2 Thickness measurement**. Due to the small thickness of the films, profilometry was initially used to determine the thickness. The results indicated that despite all the films being spun coat at the same speed, there were large deviations in film thickness. To accelerate the rate of testing, an alternate measuring method was sought out. To that end a micrometer was used on the originally measured samples to validate the results from profilometry. This allowed each individual sample to have its thickness measured before undergoing its specific test. Table 3 contains a summary of tested film thicknesses.

Table 3

*Profilometry results of polymer nanocomposite films*

| | Thickness (µm) | |
|---|---|---|
| **Sample** | **Trial 1** | **Trial 2** |
| | 10% nanoparticle | |
| Sample 1 | 22 | 24.2 |
| Sample 2 | 18.7 | 24.7 |
| | 2% nanoparticle | |
| Sample 1 | 27.7 | 29.2 |
| Sample 2 | 30.8 | 34.6 |
| | 3% nanoparticle | |
| Sample 1 | 38.1 | 34.1 |
| Sample 2 | 29.4 | 34.5 |

### 5.2 Mechanical Characterization

The prepared thin films were tested in a SHIMPO MTS to determine their Young's modulus and ultimate tensile strength. The specimens were clamped between an actuating force gauge and a stationary ground clamp, as shown in Figure 22. The sample is then pulled apart and the force vs. displacement data are collected.

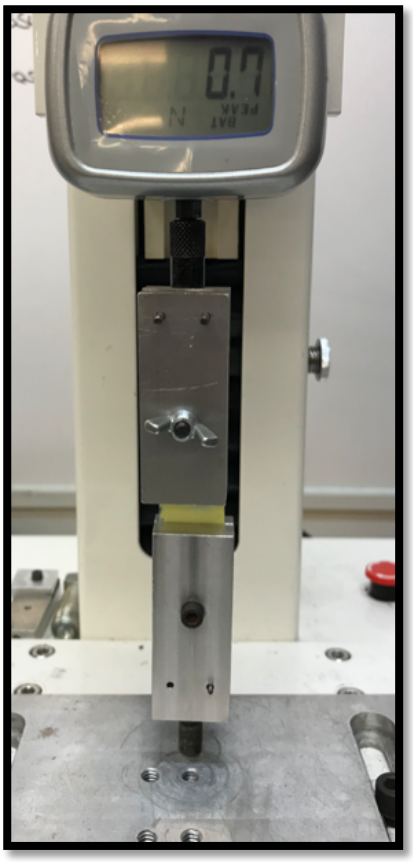


*Figure 20.* Polyimide-$SiO_2$ nanocomposite undergoing tensile testing.

Taking the sample dimensions into calculation, the force and displacement data can be converted to stress and strain values. By plotting these values against each other, stress-strain curves are obtained, examples of which are provided in Figure 21. Stress-strain curves contain valuable critical information such as Young's modulus and ultimate tensile strength. These specific curves had tensile strengths of 26.64 MPa (Figure 21a, pure polyimide), 24.5 MPa (Figure 21b, 10-wt% nanocomposite), and 9.12 MPa (Figure 21c, 15-wt% nanocomposite).

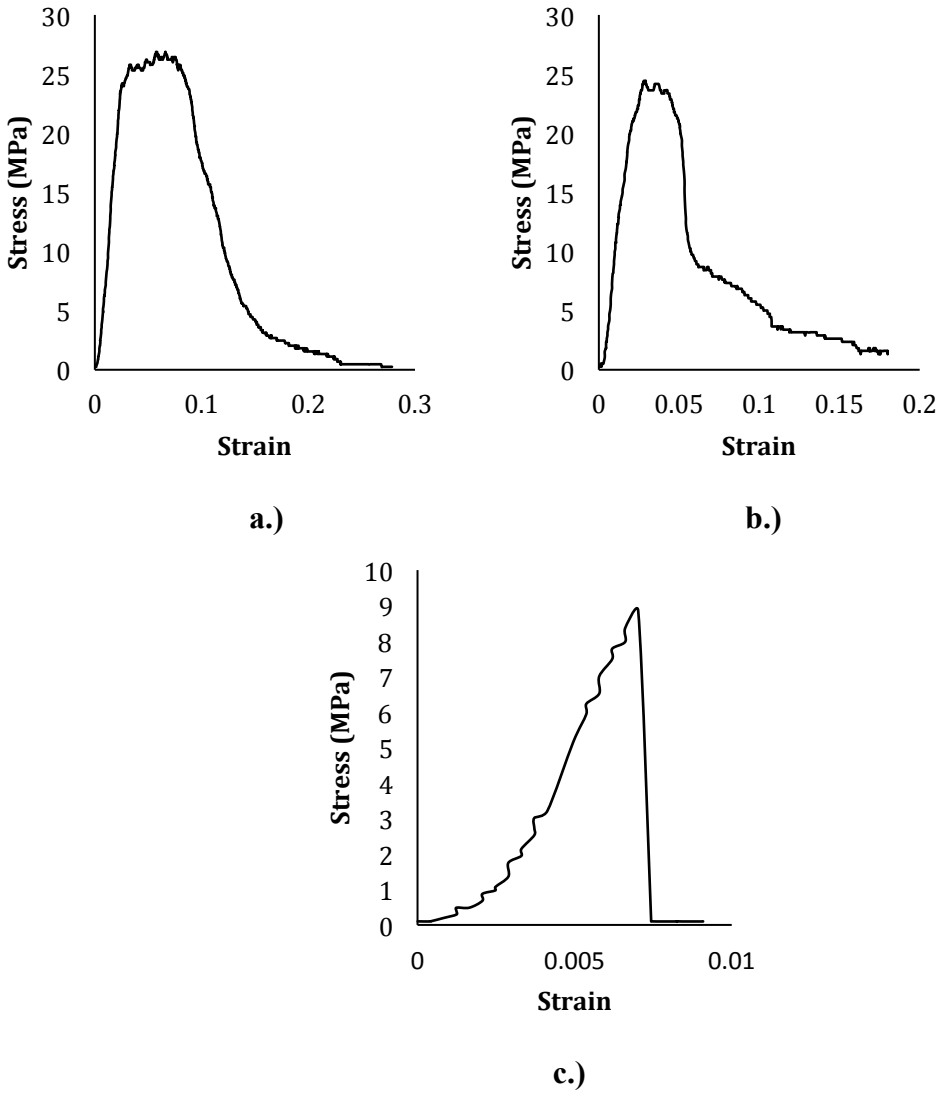


*Figure 21.* Examples of stress-strain curves of three samples. a.) 0% nanoparticle concentration, b.) 10% nanoparticle concentration, and c.) 15% nanoparticle concentration.

Pure polyimide exhibited the highest average ultimate tensile strength of 29.77 MPa. Samples with a 10% nanoparticle showed a reduced tensile strength of 24.42 MPa and the samples with a 15% concentration had a further reduced strength of 13.31 MPa. This can be explained by potential stress concentration around the particles. Figure 22

shows a box plot comparing the ultimate tensile strengths of the tested films.

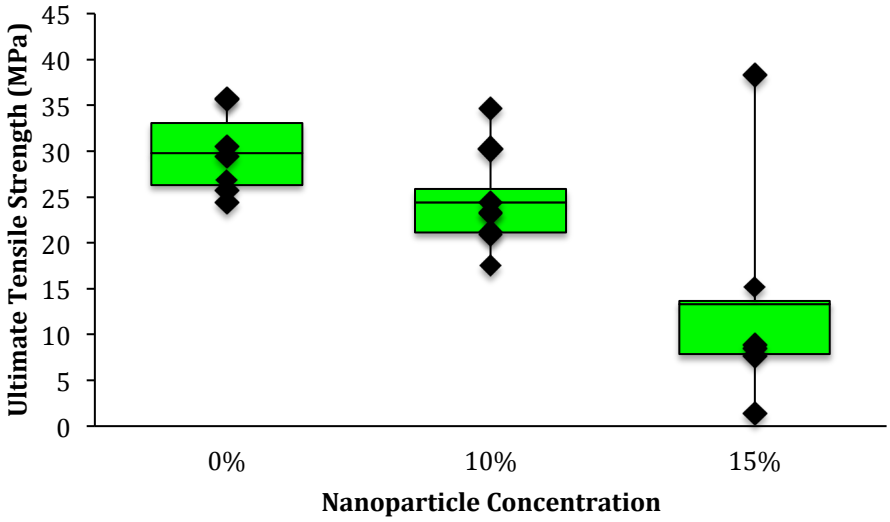


*Figure 22.* Box plot comparing ultimate tensile strengths of tested recipes.

Additionally the Young's moduli of the films were calculated. The 0% nanoparticle samples yielded an average Young's modulus of 629.4 MPa. The value increased to 841.35 MPa in 10% concentration samples, but suffered a reduction down to 587.22 MPa in 15% samples. This is in line with other observations that nanomaterial fill increases the Young's modulus at low concentrations and decreases it at higher concentrations [67, 68]. Figure 23 shows a comparison of Young's moduli for the various samples.

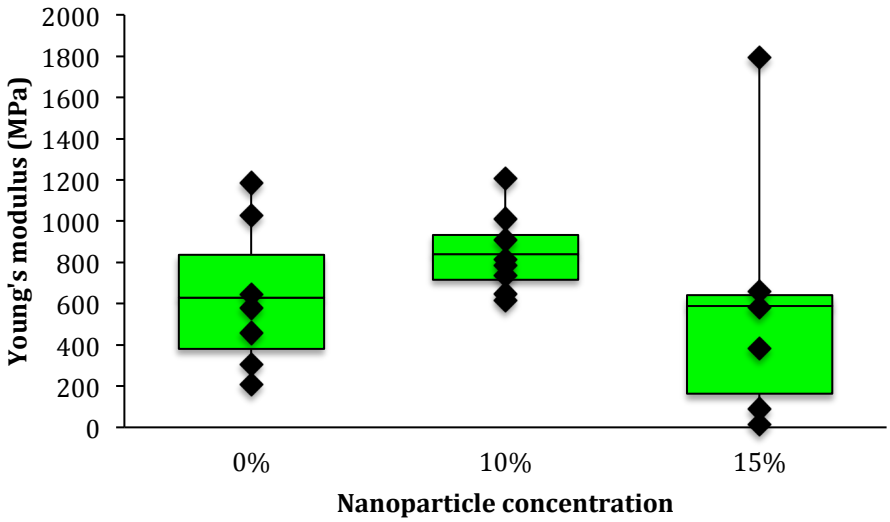


*Figure 23.* Box plot comparing Young's Modulus of tested recipes.

### 5.3 Electrical Characterization

To determine the dielectric strength of the material, a Vitrek 955i Hi-Pot testing system was used, as pictured in Figure 24. The system had a built-in safety feature to determine the exact voltage at which the material fails. Two wires from the system are attached to the electrodes that are contained within a 3D printed safety enclosure. The testing sample is then sandwiched between the electrodes and the voltage is increased from 0 V at a rate of 500 V/s until a current spike is detected. Once this occurs material breakdown is achieved, the voltage is recorded and the system ceases to apply electricity.

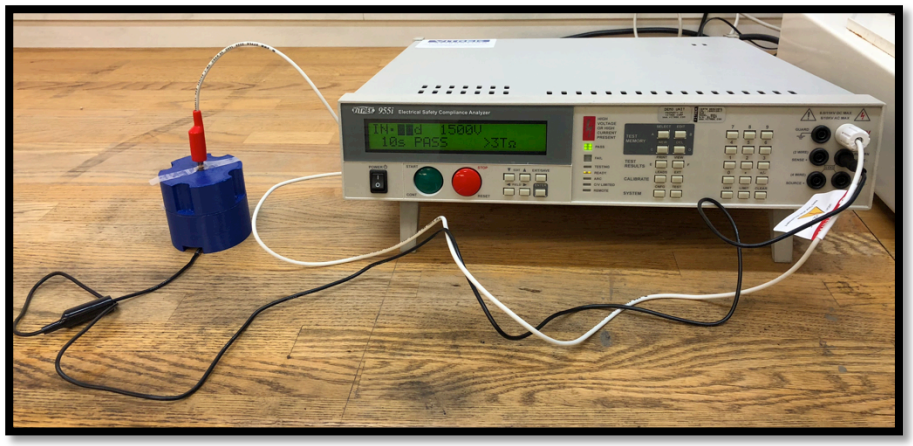


*Figure 24*. Vitrek 955i Hi-pot tester attached to a 3D printed safety enclosure.

Testing was conducted on three different sample concentrations, 0%, 10%, and 15% in nanoparticle weight percentages. Base polyimide had the highest average dielectric strength of 86.8 kV/mm. The 10% nanoparticle concentration samples and the 15% concentration had average dielectric breakdown values of 34.0 kV/mm and 40.6 kV/mm, respectively, as shown in Figure 25. The decrease in the breakdown voltage as nanoparticle concentration increases is backed up by the fact that polyimide has a higher dielectric strength than $SiO_2$ [57, 63].

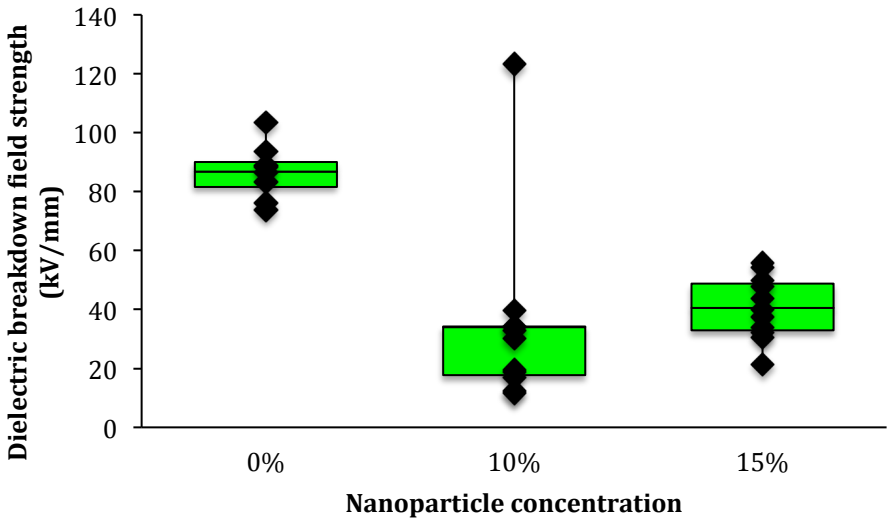


*Figure 25.* Box plot of dielectric breakdown strength of 0%, 10%, and 15% in-situ samples.

### 5.4 Conclusions

Due to the rough surface topography in ex-situ samples, we decided to pursue in-situ samples and use them for mechanical and electrical characterization. The mechanical testing data show an interesting effect where a dramatic change in properties at approximately 10% nanoparticle concentration can be observed. This is evidenced by comparable ultimate tensile strengths shown by 0% and 10% nanoparticle concentration samples with a 50% reduction in 15% samples. The 15% samples also show a large decrease in Young's modulus compared to the other two groups of samples. It is suspected that as the nanoparticle concentration increases, the properties of these filler materials becomes more critical, and eventually become the dominant factors over the bulk material properties. More research will be needed to quantify the effects of

nanoparticle concentrations in the composite properties. Both nanocomposites samples experienced electrical breakdown failure at a reduced value compared to the 0% samples. The 10% sample failed at 34.0 kV/mm and the 15% sample failed at 40.6 kV/mm, on average. Some prior research suggest that 10% may in fact be the particle concentration limit at which properties undergo a dramatic change, but it varies from material to material [69].

# Chapter 6

## Design of a Cryogenic Testing System

### 6.1 Introduction

The very nature of testing for CTE requires the ability to elevate and reduce temperatures in a controlled manner. The CTE testing is typically supported by modern refrigeration and heating systems to study material behaviors within a temperature range. However advanced heating/cooling systems are needed in cryogenic materials research, as the required temperatures are not easily obtainable. To that end, a specialized system has to be designed and fabricated, to cool a chamber to approximately 40 °K using gaseous helium.

Due to the corrosive nature of helium, care had to be taken with the choice of materials. Naturally, a helium resistant rigid material with a low heat transfer coefficient and CTE would be ideal to construct a cryochamber, as it would experience the smallest thermal impact from the outside environment. Given the material limitation and the practical standpoint, most cryochambers are made from stainless steel, such as 311 [70].

Even with proper material selection, achieving such low temperatures is no easy task. It requires four key components to operate properly together. The first of these components is a cryocooler. These coolers use powerful compressors and vacuums to create a low temperature zone on the surface of a cold head. The second critical component is a helium circulator, which moves helium through the entire system. Due to the extreme temperatures experienced by the working fluid, special pumps or fans are needed. These parts not only need to survive the extreme environment but also should cause minimal temperature effect on the working fluid. The third component is the heat

exchanger that can increase the heat transfer between the working fluid and the cold head. The fourth component is the cryochamber. This component houses the testing sample and shields them from the external environment. It ensures the desired cryogenic temperatures for the samples during testing.

### 6.2 Design

The design of the cryogenic testing system, broken down into the four main components, is shown in Figure 26. In this configuration a cryo-circulator (often a cryo fan) moves helium through a closed loop and over a heat exchanger. The heat exchanger is placed in direct contact with a cold head that has its own closed helium circuit connected to a compressor. The compressor allows the helium, and by extension the cold head, to reach cryogenic temperatures. The cold head and heat exchanger combination allows heat to be removed from the working helium in the main loop and effectively cools the loop to similar temperatures. Finally, after passing through the heat exchanger, the helium is cooled and fills the application volume, in this case the cryochamber, for sample testing.

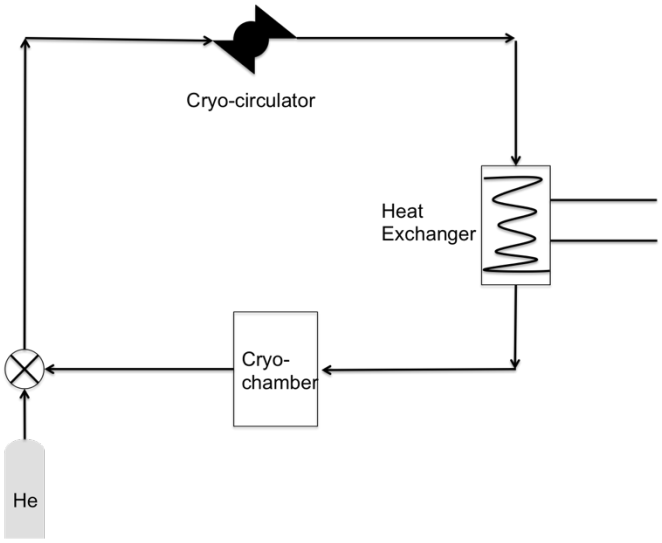


*Figure 26.* Design of the system to obtain cryogenic temperatures in the cryochamber.

**6.2.1 Helium compressor.** The Naval Surface Warfare Center, Philadelphia, to aid in the cryogenic temperature testing, loaned a helium compressor to this project. This compressor was a modified AL330 by Cryomech and was air-cooled. This compressor would not only cool the helium but also contained a helium circulator and internal heat exchanger. To connect the cryochamber to the compressor, Aeroquip flex lines with beret fittings are required. This effectively changed the system loop from the design illustrated in Figure 26 to the design shown in Figure 27.

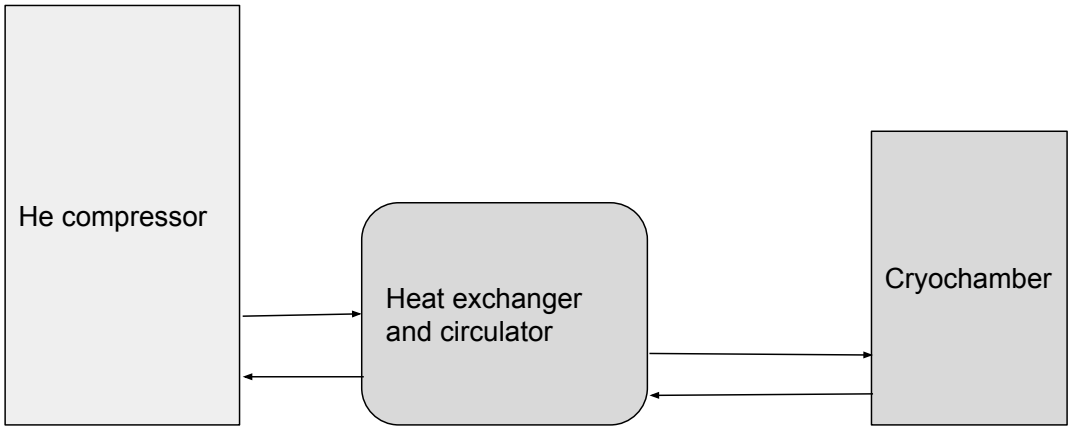


*Figure 27*. Modified cryogenic system after the Navy equipment is implemented.

**6.2.2 Cryochamber.** The cryochamber will be fabricated entirely in house; it will maintain a temperature of ~40 ºK and can be retrofitted into the existing SHIMPO MTS. Additionally it needs to be compatible with the dielectric breakdown system for electrical testing at the desired temperatures. The cryogenic testing environment has an inner diameter of 3 inches and an internal height of 7 inches, which is slightly larger than the test sample and the clamps. The chamber is separated into two parts and secured with pull action toggle clamps. The Navy partners recommended this chamber geometry. The bottom clamp is fixed, while the top clamp is suspended and adapted to interface with the SHIMPO tensile tester. At the top of the chamber, an expandable bellow allows for the SHIMPO to stress the sample while keeping the system well sealed. Figure 28 shows drawings of the designed cryogenic chamber.

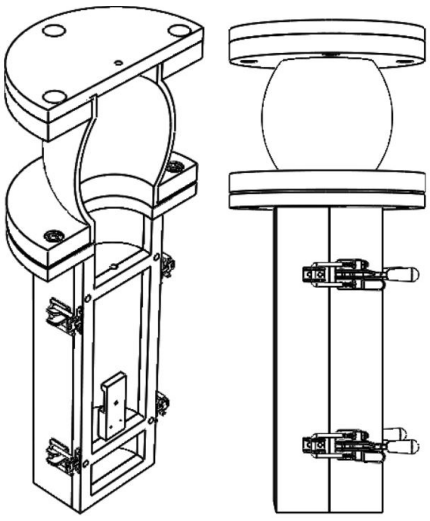

**a.)** **b.)**

*Figure 28.* a.) Isometric view of open cryochamber and b.) side view of the same chamber.

### 6.3 Discussions

The design of this chamber is to be CNC machined to establish a cylindrical geometry inside a rectangular outer vessel. To provide a suitable corrosive resistance, stainless steel 304 will be used due to its higher machinability than 311. This relatively complex geometry provides a sufficient volume of cooled helium while providing flat edges for easy sealing. Ports to attach bayonets fittings still need to be designed but can be easily added to the flat edges of the rectangular outer shell. Some forms of insulator will need to be added to maintain a cryogenic environment; for this purpose, aerogel has been heavily investigated [71-73]. This design will integrate with both the SHIMPO MTS and the Vitrek Hi-pot tester, allowing for both mechanical and electrical characterization at cryogenic temperatures. The final rendering of the cryochamber is illustrated in Figure 29.

*Figure 29.* Finished rendering of cryochamber in desired materials. A flexible bellow can be observed on top.

# Chapter 7

## Conclusions and Future Work

### 7.1 PDMS-ZnO-CNT Nanocomposite Foams

Polymer nanocomposite foams can be easily generated using an ex-situ method, combining the liquid state PDMS with ZnO and CNT nanopowders, at 10%, and 1% concentrations, respectively. This composite was then cast over dissolvable sugar scaffolds to create a porous structure.

The foams exhibit clear piezoelectric properties under mechanical deformation, with foams based upon ultrafine sugar exhibiting the largest electrical response of 0.3 V. Additionally, all the foams showed reduced mechanical strength due to the stress concentration around the pores. The ultrafine sugar had the highest strength of at 0.28 MPa. All the foams exhibited similar Young's Modulus, of 0.45 MPa, 0.50 MPa, and 0.54 MPa. These foams could be used as an energy harvester or as a potential sensor material. In terms of energy harvesting, this material has great potential to be used in the insoles of sneakers. This would allow for potential charging of mobile devices by the mechanical work from users.

The biggest issues that arise from the scaffolding methods are phase separation and particle aggregation. Due to the liquid nature of the host polymer, particles infused during the ex-situ method tend to float on top of the host matrix. A thorough mixing is challenging for viscous fluids such as the PDMS. The hand mixing of the materials also exacerbates the problem of particle aggregation.

### 7.2 Polyimide-$SiO_2$ Nanocomposite Dielectrics

Polymer nanocomposites can display many unique properties, dependent on the host matrix and the chosen nanofiller. These properties can be dramatically different from those of the base materials. Furthermore, some nanomaterials can imbue multiple material properties; for example, $SiO_2$ nanoparticles are both dielectric and useful to increase the material stability at cryogenic temperatures.

Three different nanoparticle concentrations were tested for this study: 0%, 10% and 15%. At 0% nanoparticle concentration, the samples had an electrical breakdown value of 86.6 kV/mm, while 10% and 15% samples suffered reduced strengths of 43 kV/mm and 44.6 kV/mm, respectively. A similar effect also occurred when comparing the mechanical strengths of the generated materials. The 0% concentration sample exhibited an ultimate tensile strength of 29.77 MPa. This value was reduced in 10% samples to 24.42 MPa and even reduced further to 13.31 MPa in 15% samples.

The unique material properties of composites would enable numerous applications in various areas. The $SiO_2$ nanocomposite has the potential to significantly increase the energy capacity in current superconducting systems. There are numerous benefits to such a breakthrough, specifically for the Navy. For example, such technology could aid in the adoption of rail guns, degaussing systems, and boost power transfer in Naval vessels [74, 75].

### 7.3 Future Work on PDMS-ZnO-CNT Nanocomposite Foams

While the PDMS-ZnO-CNT foams produced electricity, the voltage output value was relatively low and the electric current was not recorded. For the electric voltage

alone, it is still not enough to be harvested using circuitry, as approximately 0.7 V is required to activate the diodes in such a circuit. One potential method to increase the electric output is to use dipole alignment, where piezoelectric elements are subjected to a high electric field until the dipoles all face the same direction [76, 77]. As electricity is generated in the direction of the dipole, aligning them eliminates current cancellation and improves the overall voltage. Figure 30 illustrates this process of dipole alignment, called electric poling.

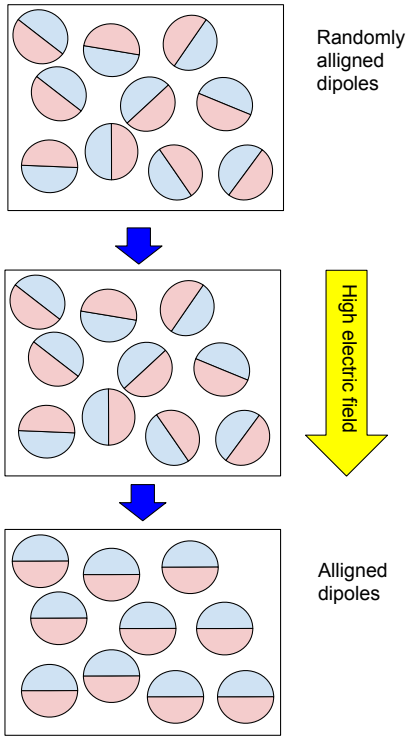


*Figure 30.* A diagram illustrating dipole alignment, in which a high electric field causes the dipoles to rotate and follow the field direction.

Another way to potentially improve the voltage is to generate foams that can experience larger deformation, without increasing the overall amount of material in the specimen. This would involve utilizing other foaming methods, other than sugar scaffolding, to create the foamed structures. Citric acid, azodicarbonamide and sodium bicarbonate are all used in industry to generate various foamed structures, and can potentially be used in this project to create piezoelectric composite foams [78]. Finally electric current measurements need to be performed, so the electrical power generated from a singular foam sample can be determined.

### 7.4 Future Work on $SiO_2$ Nanocomposite Dielectrics

For the $SiO_2$ nanocomposite there is a lot of work to be done in the future. The most urgent issue to be resolved is the implementation of the cryosystem to allow for cryogenic testing, as illustrated in Figure 31. This includes the machining of the chamber discussed in Chapter 6. As of now, all the gathered results were obtained at room temperature. Additionally, CTE testing requires a specific tool known as a dilatometer, which is not readily available. To solve this problem, we have been investigating a double extensometer method in addition to attempting to obtain a dilatometer [79, 80].

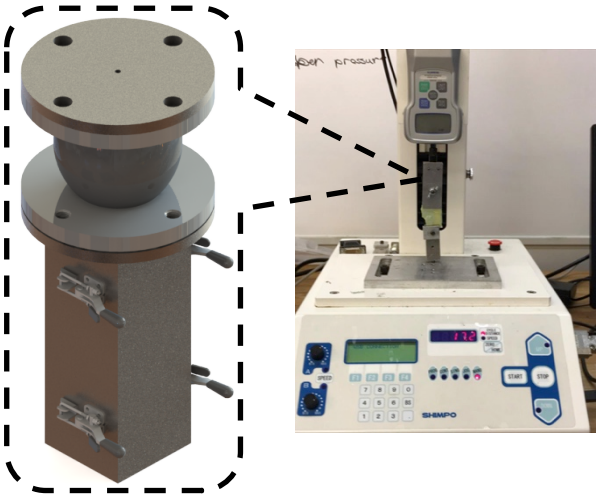

*Figure 31*. Theoretical placement of cryochamber in conjunction with the SHIMPO MTS.

## References


[1] F. C. Frary, "Research on Metals and Alloys," *Industrial & Engineering Chemistry,* vol. 26, pp. 281-284, 1934/03/01 1934.

[2] J. A. Lemire, J. J. Harrison, and R. J. Turner, "Antimicrobial activity of metals: mechanisms, molecular targets and applications," *Nature Reviews Microbiology,* vol. 11, p. 371, 05/13/online 2013.

[3] O. Tegus, E. Brück, K. H. J. Buschow, and F. R. de Boer, "Transition-metal-based magnetic refrigerants for room-temperature applications," *Nature,* vol. 415, p. 150, 01/10/online 2002.

[4] H. Kim, "Atomic layer deposition of metal and nitride thin films: Current research efforts and applications for semiconductor device processing," *Journal of Vacuum Science & Technology B: Microelectronics and Nanometer Structures Processing, Measurement, and Phenomena,* vol. 21, pp. 2231-2261, 2003/11/01 2003.

[5] J. Wu, H. Cheng, X. Xu, Y. Zhou, D. He, and Y. Liu, "Preparation and characterization of Andalusite ceramic used for solar thermal power generation," *Journal of Wuhan University of Technology-Mater. Sci. Ed.,* vol. 29, pp. 422-427, 2014/06/01 2014.

[6] M. John, "Advanced ceramic materials for next-generation nuclear applications," *IOP Conference Series: Materials Science and Engineering,* vol. 18, p. 162001, 2011.

[7] G. Moad, E. Rizzardo, and S. H. Thang, "Radical addition–fragmentation chemistry in polymer synthesis," *Polymer,* vol. 49, pp. 1079-1131, 2008/03/03/ 2008.

[8] T. Xu, N. Scafa, L.-P. Xu, L. Su, C. Li, S. Zhou*, et al.*, "Electrochemical Sensors for Nitric Oxide Detection in Biological Applications," *Electroanalysis,* vol. 26, pp. 449-468, 2014.

[9] G. Schwartz, B. C. K. Tee, J. Mei, A. L. Appleton, D. H. Kim, H. Wang*, et al.*, "Flexible polymer transistors with high pressure sensitivity for application in electronic skin and health monitoring," *Nature Communications,* vol. 4, p. 1859, 05/14/online 2013.

[10] H.-Y. Chen, J. Hou, S. Zhang, Y. Liang, G. Yang, Y. Yang*, et al.*, "Polymer solar cells with enhanced open-circuit voltage and efficiency," *Nature Photonics,* vol. 3, p. 649, 11/01/online 2009.

[11] T. C. Triantafillou and N. Plevris, "Strengthening of RC beams with epoxy-bonded fibre-composite materials," *Materials and Structures,* vol. 25, pp. 201-211, 1992/05/01 1992.

[12] R.P.LNijssn, *Composite Materials An Introduction*: VKCN, 2015.

[13] B.-S. Lim, J. L. Ferracane, J. R. Condon, and J. D. Adey, "Effect of filler fraction and filler surface treatment on wear of microfilled composites," *Dental Materials,* vol. 18, pp. 1-11, 2002.

[14] R. C. Neagu, E. K. Gamstedt, and F. Berthold, "Stiffness Contribution of Various Wood Fibers to Composite Materials," *Journal of Composite Materials,* vol. 40, pp. 663-699, 2006/04/01 2005.

[15] "Diamonds and the Geology of Mantle Carbon," *Reviews in Mineralogy and Geochemistry,* vol. 75, pp. 355-421, 2013.

[16] J. Z. Zhang, D. Simionesie, and C. Schaschke, "Graphite and Hybrid Nanomaterials as Lubricant Additives," *Lubricants,* vol. 2, 2014.

[17] A. Hirsch, "Functionalization of Single-Walled Carbon Nanotubes," *Angewandte Chemie International Edition,* vol. 41, pp. 1853-1859, 2002.

[18] H. Terrones, M. Terrones, E. Hernández, N. Grobert, J. C. Charlier, and P. M. Ajayan, "New Metallic Allotropes of Planar and Tubular Carbon," *Physical Review Letters,* vol. 84, pp. 1716-1719, 02/21/ 2000.

[19] W. A. Zinzow and T. Hazen, "Electrical Properties of Certain Bakelite Materials," *Industrial & Engineering Chemistry,* vol. 27, pp. 899-902, 1935/08/01 1935.

[20] A. C. Balazs, T. Emrick, and T. P. Russell, "Nanoparticle Polymer Composites: Where Two Small Worlds Meet," *Science,* vol. 314, pp. 1107-1110, 2006.

[21] A. Usuki, Y. Kojima, M. Kawasumi, A. Okada, Y. Fukushima, T. Kurauchi*, et al.*, "Synthesis of nylon 6-clay hybrid," *Journal of Materials Research,* vol. 8, pp. 1179-1184, 2011.

[22] P. Giannelis Emmanuel, "Polymer Layered Silicate Nanocomposites," *Advanced Materials,* vol. 8, pp. 29-35, 1996/01/01 1996.

[23] S. Chatterjee and A. Basu, *Challenges in Manufacturing Aluminium Based Metal Matrix Nanocomposites via Stir Casting Route* vol. 736, 2013.

[24] A. Prasad Reddy, P. Vamsi Krishna, R. Narasimha Rao, and N. V. Murthy, "Silicon Carbide Reinforced Aluminium Metal Matrix Nano Composites-A Review," *Materials Today: Proceedings,* vol. 4, pp. 3959-3971, 2017/01/01/ 2017.

[25] N. Van Hieu, L. T. B. Thuy, and N. D. Chien, "Highly sensitive thin film NH3 gas sensor operating at room temperature based on SnO2/MWCNTs composite," *Sensors and Actuators B: Chemical,* vol. 129, pp. 888-895, 2/22/ 2008.

[26] R. Najjar, Y. Luo, X. Hu, V. Beachley, and W. Xue, "Study of energy harvesting performance of wet-stretched PVDF nanofibers," presented at the The ASME 2016 International Mechanical Engineering Congress & Exposition (ASME IMECE 2016), Phoenix, AZ, USA, 2016.

[27] E. L. Mayes, F. Vollrath, and S. Mann, "Fabrication of Magnetic Spider Silk and Other Silk-Fiber Composites Using Inorganic Nanoparticles," *Advanced Materials,* vol. 10, pp. 801-805, 1998.

[28] Y. Lalatonne, J. Richardi, and M. P Pileni, *Van der Waals versus dipolar forces controlling mesoscopic organizations of magnetic nanocrystals* vol. 3, 2004.

[29] Q. Guo, R. Ghadiri, T. Weigel, A. Aumann, E. Gurevich, C. Esen*, et al.*, "Comparison of in Situ and ex Situ Methods for Synthesis of Two-Photon Polymerization Polymer Nanocomposites," *Polymers,* vol. 6, p. 2037, 2014.

[30] X. Chen, S. Wei, A. Yadav, R. Patil, J. Zhu, R. Ximenes*, et al.*, "Poly(propylene)/Carbon Nanofiber Nanocomposites: Ex Situ Solvent-Assisted Preparation and Analysis of Electrical and Electronic Properties," *Macromolecular Materials and Engineering,* vol. 296, pp. 434-443, 2011.

[31] J. Baur and E. Silverman, "Challenges and Opportunities in Multifunctional Nanocomposite Structures for Aerospace Applications," *MRS Bulletin,* vol. 32, pp. 328-334, 2011.

[32] S. H. Ng, J. Wang, D. Wexler, K. Konstantinov, Z. P. Guo, and H. K. Liu, "Highly Reversible Lithium Storage in Spheroidal Carbon‐Coated Silicon Nanocomposites as Anodes for Lithium‐Ion Batteries," *Angewandte Chemie International Edition,* vol. 45, pp. 6896-6899, 2006.

[33] D. Feldman, "Polymer nanocomposites in medicine," *Journal of Macromolecular Science, Part A,* vol. 53, pp. 55-62, 2016/01/02 2016.

[34] H. W. Kim, J. H. Song, and H. E. Kim, "Bioactive glass nanofiber–collagen nanocomposite as a novel bone regeneration matrix," *Journal of Biomedical Materials Research Part A,* vol. 79A, pp. 698-705, 2006.

[35] J. Selvarathinam and A. Anpalagan, "Energy Harvesting From the Human Body for Biomedical Applications," *IEEE Potentials,* vol. 35, pp. 6-12, 2016.

[36] J. R. Nalbach, D. Jao, D. G. Petro, K. M. Raudenbush, S. Ahmad, Y. Xue*, et al.*, "Fabrication of tunable silk materials through microfluidic mixers," presented at the ASME 2016 International Mechanical Engineering Congress & Exposition (ASME IMECE 2016), Phoenix, AZ, USA, 2016.

[37] S. Hardt, H. Pennemann, and F. Schönfeld, "Theoretical and experimental characterization of a low-Reynolds number split-and-recombine mixer," *Microfluidics and Nanofluidics,* vol. 2, pp. 237-248, 2005.

[38] W. R. McCall, C. Kim K Fau - Heath, G. Heath C Fau - La Pierre, D. J. La Pierre G Fau - Sirbuly, and D. J. Sirbuly, "Piezoelectric nanoparticle-polymer composite foams," 20141126 DCOM- 20151023.

[39] D. N. H. Tran, S. Kabiri, T. R. Sim, and D. Losic, "Selective adsorption of oil-water mixtures using polydimethylsiloxane (PDMS)-graphene sponges," *Environmental Science: Water Research & Technology,* vol. 1, pp. 298-305, 2015.

[40] C. N. R. Rao, B. C. Satishkumar, A. Govindaraj, and M. Nath, "Nanotubes," *ChemPhysChem,* vol. 2, pp. 78-105, 2001.

[41] T. Ando, H. Matsumura, and T. Nakanishi, "Theory of ballistic transport in carbon nanotubes," *Physica B: Condensed Matter,* vol. 323, pp. 44-50, 2002/10/01/ 2002.

[42] D. Sinton, "Energy: the microfluidic frontier," *Lab on a Chip,* vol. 14, pp. 3127-3134, 2014.

[43] E. Lefeuvre, A. Badel, C. Richard, L. Petit, and D. Guyomar, "A comparison between several vibration-powered piezoelectric generators for standalone systems," *Sensors and Actuators A: Physical,* vol. 126, pp. 405-416, 2/14/ 2006.

[44] J. M. Donelan, Q. Li, V. Naing, J. A. Hoffer, D. J. Weber, and A. D. Kuo, "Biomechanical energy harvesting: generating electricity during walking with minimal user effort," *Science,* vol. 319, pp. 807-810, 2008.

[45] L. Xie, J. Li, S. Cai, and X. Li, "Design and experiments of a self-charged power bank by harvesting sustainable human motion," *Advances in Mechanical Engineering,* vol. 8, p. 1687814016651371, 2016.

[46] K. J. Loh and D. Chang, "Zinc oxide nanoparticle-polymeric thin films for dynamic strain sensing," *Journal of Materials Science,* vol. 46, pp. 228-237, 2011// 2011.

[47] X.-Q. Fang, J.-X. Liu, and V. Gupta, "Fundamental formulations and recent achievements in piezoelectric nano-structures: a review," *Nanoscale,* vol. 5, pp. 1716-1726, 2013.

[48] R. A. Hawsey and S. Morozumi, "The Energy and Environmental Benefits of Superconducting Power Products," *Mitigation and Adaptation Strategies for Global Change,* vol. 10, pp. 279-306, 2005/04/01 2005.

[49] J. Nagamatsu, N. Nakagawa, T. Muranaka, Y. Zenitani, and J. Akimitsu, "Superconductivity at 39 K in magnesium diboride," *Nature,* vol. 410, p. 63, 03/01/online 2001.

[50] R. J. Cava, H. Takagi, H. W. Zandbergen, J. J. Krajewski, W. F. Peck Jr, T. Siegrist*, et al.*, "Superconductivity in the quaternary intermetallic compounds LnNi2B2C," *Nature,* vol. 367, p. 252, 01/20/online 1994.

[51] J. Maguire, A. Allais, J. Yuan, F. Schmidt, F. Hamber, and W. Tom, "Fault Management of a Cold Dielectric HTS Power Transmission Cable," *Journal of Physics: Conference Series,* vol. 43, p. 853, 2006.

[52] V. Ravi, S. Firdosy, T. Caillat, E. Brandon, K. Van Der Walde, L. Maricic*, et al.*, "Thermal Expansion Studies of Selected High-Temperature Thermoelectric Materials," *Journal of Electronic Materials,* vol. 38, pp. 1433-1442, 2009/07/01 2009.

[53] H. Kwok, K. Briggs, and V. Tabard-Cossa, "Nanopore Fabrication by Controlled Dielectric Breakdown," *PLOS ONE,* vol. 9, p. e92880, 2014.

[54] E. B. Forsyth, "The dielectric insulation of superconducting power cables," *Proceedings of the IEEE,* vol. 79, pp. 31-40, 1991.

[55] A. J. Pearmain, M. Kosaki, and R. Thomas, "Partial discharge performance of lapped plastic insulation for superconducting power transmission cables and the dielectric strength of supercritical helium gas," *Conference on Electrical Insulation & Dielectric Phenomena - Annual Report 1978,* pp. P 382-389, 1978.

[56] L. Graber, W. J Kim, P. Cheetham, C. Kim, H. Rodrigo, and S. Pamidi, *Dielectric Properties of Cryogenic Gas Mixtures Containing Helium, Neon, and Hydrogen* vol. 102, 2015.

[57] W. M. Haynes, *CRC handbook of chemistry and physics: A ready-reference book of chemical and physical data*, 6th ed. Boca Raton: CRC Press, 2009.

[58] E. Tuncer, A. J. Rondinone, J. Woodward, I. Sauers, D. R. James, and A. R. Ellis, "Cobalt iron-oxide nanoparticle modified poly(methyl methacrylate) nanodielectrics," *Applied Physics A,* vol. 94, pp. 843-852, 2009/03/01 2009.

[59] C. J. Huang, S. Y. Fu, Y. H. Zhang, B. Lauke, L. F. Li, and L. Ye, "Cryogenic properties of SiO2/epoxy nanocomposites," *Cryogenics,* vol. 45, pp. 450-454, 2005/06/01/ 2005.

[60] G. Polizos, E. Tuncer, I. Sauers, D. R. James, A. R. Ellis, and K. L. More, "ELECTRICAL AND MECHANICAL PROPERTIES OF TITANIUM DIOXIDE NANOPARTICLE FILLED EPOXY RESIN COMPOSITES," *AIP Conference Proceedings,* vol. 1219, pp. 41-46, 2010/04/08 2010.

[61] X.-G. Chen, J.-D. Guo, B. Zheng, Y.-Q. Li, S.-Y. Fu, and G.-H. He, "Investigation of thermal expansion of PI/SiO2 composite films by CCD imaging technique from −120 to 200°C," *Composites Science and Technology,* vol. 67, pp. 3006-3013, 2007/11/01/ 2007.

[62] T. Enis, S. Isidor, D. R. James, R. E. Alvin, M. P. Paranthaman, A. Tolga*, et al.*, "Electrical properties of epoxy resin based nano-composites," *Nanotechnology,* vol. 18, p. 025703, 2007.

[63] S. M. Sobhan Niyogi, Basudam Adhikari, "Mechanical and electrical properties of polyimide blend films," *Indian Journal of Chemical Technology,* vol. 8, 28 November 2000 2000.

[64] Y. Zhou, Y. Bai, K. Yu, Y. Kang, and H. Wang, "Excellent thermal conductivity and dielectric properties of polyimide composites filled with silica coated self-passivated aluminum fibers and nanoparticles," *Applied Physics Letters,* vol. 102, p. 252903, 2013/06/24 2013.

[65] E. Tuncer, I. Sauers, D. R. James, A. R. Ellis, and R. C. Duckworth, "Nanodielectric system for cryogenic applications: Barium titanate filled polyvinyl alcohol," *IEEE Transactions on Dielectrics and Electrical Insulation,* vol. 15, pp. 236-242, 2008.

[66] Y.-J. Kim, J.-H. Kim, S.-W. Ha, D. Kwon, and J.-K. Lee, "Polyimide nanocomposites with functionalized SiO2 nanoparticles: enhanced processability, thermal and mechanical properties," *RSC Advances,* vol. 4, pp. 43371-43377, 2014.

[67] C. Feng, Y. Wang, S. Kitipornchai, and J. Yang, "Effects of Reorientation of Graphene Platelets (GPLs) on Young's Modulus of Polymer Nanocomposites under Uni-Axial Stretching," *Polymers,* vol. 9, 2017.

[68] S. N. Raja, A. J. Luong, W. Zhang, L. Lin, R. O. Ritchie, and A. P. Alivisatos, "Cavitation-Induced Stiffness Reductions in Quantum Dot–Polymer Nanocomposites," *Chemistry of Materials,* vol. 28, pp. 2540-2549, 2016/04/26 2016.

[69] M. S. Islam, R. Masoodi, and H. Rostami, "The Effect of Nanoparticles Percentage on Mechanical Behavior of Silica-Epoxy Nanocomposites," *Journal of Nanoscience,* vol. 2013, p. 10, 2013.

[70] E. G. Kendall, "Metals and Alloys for Cryogenic Applications- A Review," S. S. Division, Ed., ed. Inglewood California, 1964.

[71] K. Kim, H. Kang, S. Shin, H. Oh In, C. Son, H. Cho Yun*, et al.*, "Composite aerogel insulation for cryogenic liquid storage," *IOP Conference Series: Materials Science and Engineering,* vol. 171, p. 012093, 2017.

[72] J. E. Fesmire, J. B. Ancipink, A. M. Swanger, S. White, and D. Yarbrough, "Thermal conductivity of aerogel blanket insulation under cryogenic-vacuum conditions in different gas environments," *IOP Conference Series: Materials Science and Engineering,* vol. 278, p. 012198, 2017.

[73] P. C. Thapliyal and K. Singh, "Aerogels as Promising Thermal Insulating Materials: An Overview," *Journal of Materials,* vol. 2014, p. 10, 2014.

[74] B. K. Fitzpatrick, E. M. Golda, and J. T. Kephart, "HIGH TEMPERATURE SUPERCONDUCTING DEGAUSSING–COOLING TWO HTS COILS WITH ONE CRYOCOOLER FOR THE LITTORAL COMBAT SHIP," *AIP Conference Proceedings,* vol. 985, pp. 277-283, 2008/03/16 2008.

[75] J. T. Kephart, B. K. Fitzpatrick, P. Ferrara, M. Pyryt, J. Pienkos, and E. Michael Golda, *High Temperature Superconducting Degaussing From Feasibility Study to Fleet Adoption* vol. 21, 2011.

[76] Y. Lee Keun, D. Kim, J. H. Lee, Y. Kim Tae, K. Gupta Manoj, and S. W. Kim, "Unidirectional High‐Power Generation via Stress‐Induced Dipole Alignment from ZnSnO3 Nanocubes/Polymer Hybrid Piezoelectric Nanogenerator," *Advanced Functional Materials,* vol. 24, pp. 37-43, 2013.

[77] G. M. Sessler, "Piezoelectricity in polyvinylidenefluoride," *The Journal of the Acoustical Society of America,* vol. 70, pp. 1596-1608, 1981/12/01 1981.

[78] P. S. Garcia, M. V. E. Grossmann, F. Yamashita, S. Mali, L. H. Dall'Antonia, and W. J. Barreto, "Citric acid as multifunctional agent in blowing films of starch/PBAT," *Química Nova,* vol. 34, pp. 1507-1510, 2011.

[79] M. J. Dedicatoria, J. R. Dizon, H.-S. Shin, and K.-D. Sim, *Establishment of CTE Measurement Procedure for PPLP at 77 K for HTS Power Cables using Double Extensometers* vol. 14, 2012.

[80] S. Ran, C. T. Wolowiec, I. Jeon, N. Pouse, N. Kanchanavatee, B. D. White*, et al.*, "Phase diagram and thermal expansion measurements on the system URu2−xFexSi2," *Proceedings of the National Academy of Sciences,* vol. 113, p. 13348, 2016.